UNIVERSITÀ DEGLI STUDI DI TORINO

Doctoral School in Life and Health Sciences

PhD in Medical Pathophysiology

IL-3R-alpha blockade inhibits tumor endothelial cell-derived extracellular vesicle (EV)-mediated vessel formation by targeting the β-catenin pathway.

Coordinator

Prof. Giovanni Camussi

Prof. Franco Veglio

Scientific Supervisor **Candidate**

Prof.ssa Maria Felice Brizzi **Giusy Lombardo**

XXX CYCLE

ABSTRACT

The proangiogenic cytokine Interleukin 3 (IL-3) is released by inflammatory cells in breast and ovarian cancer tissue microenvironments and also acts as an autocrine factor for human breast and kidney-Tumor-derived Endothelial Cells (TECs). We have previously shown that IL-3-treated endothelial cells (ECs) release extracellular vesicles (EVs), which serve as a paracrine mechanism for neighboring ECs, by transferring active molecules. The impact of an anti-IL-3R-alpha blocking antibody on the proangiogenic effect of EVs released from TECs (anti-IL-3R-EVs) has therefore been investigated in this study. We have found that anti-IL-3R-EV treatment prevented neovessel formation and, more importantly, also induced the regression of *in-vivo* TEC-derived neovessels. Two miRs that target the canonical wingless (Wnt)/β-catenin pathway, at different levels, were found to be differentially regulated when comparing the miR-cargo of naïve TEC-derived EVs (EVs) and anti-IL-3R-EVs. miR-214-3p, which directly targets *β*-catenin, was found to be upregulated, whereas miR-24-3p, which targets adenomatous polyposis coli (APC) and glycogen synthase kinase-3β (GSK3β), was found to be downregulated. In fact, upon their transfer into the cell, low *β*-catenin content and high levels of the two members of the "*β*-catenin destruction complex" were detected. Moreover, c-myc downregulation was found in TECs treated with anti-IL-3R-EVs, pre-miR-214-3p-EVs and antago-miR-24-3p-EVs, which is consistent with network analyses of miR-214-3p and miR-24-3p gene targeting. Finally, *in-vivo* studies have demonstrated the impaired growth of vessels in pre-miR-214-3p-EV- and antago-miR-24-3p-EV-treated animals. These effects became much more evident when combo treatment was applied.

The results of the present study identify the canonical Wnt/β-catenin pathway as a relevant mechanism of TEC-derived EV pro-angiogenic action. Furthermore, we herein provide evidence that IL-3R blockade may yield some significant advantages, than miR targeting, in inhibiting the proangiogenic effects of naïve TEC-derived EVs by changing TEC-EV-miR cargo.

INTRODUCTION

Interleukin 3 and its inflammatory and pro-angiogenic actions

Interleukin 3 (IL-3) is a secreted monomeric glycoprotein originally described as a potent growth factor which acts on progenitor/stem cells and on mature cells (Greenberger et al, 1983; Metcalf et al,1986). In fact, IL-3 is a cytokine that promotes survival, proliferation, and differentiation of hemopoietic progenitor cells of several lineages including granulocytes, erythrocytes, monocytes, megakaryocytes, and lymphocytes but also modulates the activity of mature cells (Brizzi et al, 1996). IL-3 exerts its biologic activities through binding to specific high-affinity receptors on the cell surface. The human IL-3 receptor (IL-3R) consists of two subunits, a ligand-specific α chain which binds IL-3 with low affinity, and a β chain, which does not bind IL-3 by itself but confers high affinity binding capability to the receptor (Korpelainen et al, 1996).

T lymphocytes and mast cells are the most relevant IL-3-producing cells (Rothenberg et al, 1988; Ihle et al, 1992). These cells are essential mediators of normal tissue inflammatory and allergic reactions and of tissue damage in many autoimmune diseases.

Inflammation represents a critical and unifying driving force promoting atherosclerotic plaque progression. The pathogenesis of this disease has been extensively studied and can be traced to the intimal event of macrophages and lymphocytes infiltrating the arterial wall, presumably secondary to endothelial dysfunction (Ross, 1999). Moreover, T lymphocytes and macrophages are particularly abundant at the leading edge of the lesion, or the “shoulder” region, a side where the atherosclerotic plaques are more vulnerable and tend to rupture (Newby et al, 1999). This observation highlights the critical role of the T cell in this process and sustains the proposal that T cell–derived cytokines implicated in the regulation of collagen synthesis may be involved in weakening the fibrous cap. Despite connective tissue remodeling, atherosclerosis is a consequence of proliferation and directed migration of vascular smooth muscle cells (SMCs) (Ferrara et al, 1999).

Atherosclerotic lesion progression requires intraplaque neovascularization (Koenig et al, 2007; Packard et al, 2008), and the inflammatory cells contained in neointima mainly contribute to this process by releasing cytokines and growth factors, such as IL-3 and other growth factors (Brizzi et al, 2001; Koenig et al, 2007; Packard et al, 2008) as suggested by the in vivo angiogenic properties of some of these secreted factors. Moreover, as previously shown IL-3 is able to induce endothelial cell proliferation and in vivo new vessel formation as well as SMC proliferation and migration (Brizzi et al, 1993; Dentelli et al, 1999; Brizzi et al, 2001).

IL-3 and tumor angiogenesis

Angiogenesis is required for tumor development, growth, invasion and metastasis (Yancopoulos et al, 2000; Ferrara et al, 2003; Friedl and Wolf, 2003). The involvement of IL-3 in vascular cell proliferation and activation during physiological and tumor angiogenesis has been extensively documented (Dentelli et al, 2005; Zeoli et al, 2008; Dentelli et al, 2010; Uberti et al 2010; Moldenhauer et al, 2015). Tumor microenvironment consists of tumor cells that proliferate and interact with stromal cells, including endothelial cells (ECs) and inflammatory cells (Folkman et al, 1989; Rafii et al, 2002). A number of studies have shown that tumor growth depends on the rapid recruitment of ECs which contributes to functional neovasculature (Folkman et al, 1989; Carmeliet, 2003).

At this regard, we have previously shown that the inflammatory cytokine IL-3 (Dentelli et al, 1999) is released into the microenvironment of breast cancer tissues (Dentelli et al, 2004) and, consistent with the original observation that activated T-lymphocytes are the main cellular source of IL-3 (Wimperis et al, 1989), we also found that in noninvasive breast cancer tissues a subset of tumor infiltrating CD25/CD4/CD5þ T cells express IL-3 (Dentelli et al, 1999). Moreover, we have also previously shown that IL-3 is secreted by tat-expressing cells (Deregibus et al, 2002), and that, besides tumor infiltrating lymphocytes, tumor-derived ECs also represent an important source of IL-3 (Bussolati et al, 2003). IL-3, released into tumor microenvironment (Dentelli et al, 2004),

besides promoting survival and proliferation of mature endothelial cells (Brizzi et al 1993; Dentelli et al, 1999), also acts as an endothelial differentiation factor for hematopoietic derived endothelial progenitor cells (EPCs) (Zeoli et al, 2008) which actively participate to tumor vessel formation as well (Uberti et al. 2010). For a tumor to develop as a highly malignant and deadly phenotype, it has to recruit and sustain its own blood supply, a process known as tumor angiogenesis (Folkman, 2007). These vessels are newly formed from pre-existing host vessels stimulated by proangiogenic factors released by tumor cells. Hence, tumor cells establish a specific stromal microenvironment fostering tumor growth, in which angiogenesis is strongly involved (Folkman, 2007; Shchors and Evan, 2007; Kerbel, 2008). Tumor blood vessels provide nutrition and oxygen in response to demand of proliferating tumor cells and act as gatekeepers for tumor-cell escape to enter into the circulation, thus favoring metastasis (Folkman, 2007; Shchors and Evan, 2007; Kerbel, 2008). Actually, it is well established that, in term of morphology, tumor-derived endothelial cells (TECs) possess a distinct and unique phenotype compared with normal endothelial cells (NECs) (Baluk et al., 2003). A number of evidences indicate that there are differences at both molecular and functional levels. Unlike NECs in normal quiescent endothelium, TECs have a rapid turnover rate and therefore have been termed ‘activated ECs”. The ‘activated’ phenotype of TECs (Bussolati et al, 2003; Folkman, 2007) has been related to the expression of embryonic genes (St Croix et al, 2000) as well as genes regulating vessel growth, including IL-3 (Deregibus et al 2002). It has been extensively demonstrated that tumor-associated angiogenesis is sustained by a complex network of cytokines, which provide paracrine and autocrine cues to both tumor cells and stromal cells (including ECs, non-endothelial mesenchymal cells and inflammatory cells) (Butler et al, 2010). TECs have an intrinsic pro-angiogenic capability independently of tumor microenvironment but driven by their autocrine release of IL-3 (Deregibus et al 2002; Uberti et al 2010). Thus, our findings demonstrating that IL-3 may promote tumor angiogenesis and contribute to myeloid cell recruitment (Uberti et al 2010) provide the mechanistic rational to exploit IL-3 as an alternative target that, in complementary approaches, might confer a significant therapeutic advantage.

As reported by Bussolati *et al.* (Bussolati et al, 2003) IL-3 also acts as an autocrine factor for TECs. These data have been further validated in human breast and kidney TECs (Dentelli P et al, 2011). Overall, IL-3, released in the tumor microenvironment, can contribute to tumor growth via paracrine and autocrine mechanisms.

Extracellular vesicles (EVs)

The classic paracrine signaling paradigm has been re-evaluated somewhat since it was discovered that both cancer and tumor microenvironment cells generate membrane-enclosed packets, called extracellular vesicles (EVs). Cell-to-cell communication is required to guarantee proper coordination among different cell types within tissues. Cells respond to soluble factors, and also communicate by adhesion molecule mediated cell-to-cell interactions. This interaction connects neighboring cells via ligand-receptor-mediated transfer of surface-associated molecules, or by tunneling nanotubules which on turn allow the transfer of surface molecules and cytoplasmic components. Recent studies have suggested that cells may also communicate by circular membrane fragments named EVs (Camussi et al, 2010).

EVs are cytosol fragments with spheroid morphology surrounded by a membrane composed of a lipid bilayer and hydrophilic proteins, similar to the cell plasma membrane. EVs are considered a heterogeneous group of vesicles including exosomes, microvesicles (MVs)/microparticles and apoptotic bodies (Gyorgy et al, 2011). Their main characteristics are described in Table 1.

	Apoptotic Bodies	Microvesicles or Microparticles	Exosomes
Size	>1 μm	100–1000 nm	<100 nm
Formation mechanisms	Cell shrinkage and cell death	Membrane blebbing	Multivesicular bodies fusion with plasmatic membrane
Characteristics			
Contents	Cell organelles, proteins, DNA, RNA, and miRNA	Proteins, RNA, miRNA, and lipids	Proteins, RNA, and miRNA
Membrane properties	Membrane permeable (PI positive)	Membrane impermeable (PI negative)	Membrane impermeable (PI negative)
Markers	Annexin V positivity	Annexin V positivity and origin cell-specific markers	LAMP1, CD63, and TSG101, MFGE8/lactadherin
Detection methods	Flow cytometry and electron microscopy	Flow cytometry for MPs >300 nm and electron microscopy	Flow cytometry with CD68 capture, electron microscopy, Western blot for exosomes enriched markers
Size determination		NTA and DLS	

Table1. Characteristics of the Different Types of Extracellular Vesicles (Loyer X et al. 2014)

They are produced in vitro or in vivo physiologically by cells, or following the activation induced by soluble agonists, physical or chemical stress. The latter including oxidative stress and hypoxia (Tetta et al, 2013).

Released EVs may remain in the extracellular space in proximity of the cell of origin or may enter into biological fluids reaching distant sites (endocrine action). This may explain the presence of EVs in diverse body fluids including blood, plasma, urine, saliva, milk, and cerebrospinal fluid. (Colombo et al, 2014).

So far, cell-secreted EVs have emerged as an integral component of intercellular exchange of information. This concept is based on the observation that EVs may transfer different types of signals to recipient cells (Ratajczak et al, 2006). EVs carry receptors, bioactive lipids, proteins and nucleic acid, such as mRNA and micro RNA (miR). The delivery of mRNA to target cells is followed by subsequent transcription and synthesis of functional proteins. Moreover, transferred miRs may interfere with the production of target proteins within recipient cells. Consequently, EVs may modify the phenotype and functions of target cells (Tetta et al, 2012). EVs may directly activate recipient cells by acting as signaling complexes, by transferring receptors. This results in membrane proteins and lipids recycling, immune modulation, senescence, angiogenesis, cellular proliferation and differentiation. Some of these proteins are universally carried by EVs released by different cell types. They include Tumor suppressor gene 101 (Tsg101), Heat-shock protein 70 (Hsp70), and the tetraspanins CD9, CD63, and CD81. While others seem to be specific of their cell of origin.

EVs in tumor biology

In recent years, these once-neglected particles have been analyzed and their roles in many cellular functions, particularly in cancer, have been demonstrated. In particular, EVs released from

cancer cells contain proteins reflecting their endosomal origin together with cellular oncogenic drivers, phosphorylated proteins and miRs (Valadi et al, 2007; Tickner et al, 2014; Penfornis et al, 2016).

EVs have multiple roles in tumorigenesis: EVs released from tumor cells can affect the local tumor microenvironment, the extracellular matrix remodeling, and also promote vasculogenesis and tumor cell proliferation. They also move to distant sites to promote the generation of the pre-metastatic niche. Vascularization is augmented in sites where endothelial and stromal cell differentiation is induced, leading to a pro-tumor environment. Furthermore immune responses become deregulated so that tumor recognition and anti-tumor immune functions became hampered. On the other hand, circulating tumour cell-derived EVs induce cytotoxic T-cell apoptosis, T-helper cell differentiation toward a T-regulatory cell phenotype, and impair NK cell proliferation. As a consequence bone-marrow-derived cells are recruited to tumors and pre-tumor tissues and contribute to cancer development (Tickner JA et al, 2014) (Figure 1). Therefore, to inhibiting EV functional effects would most likely yield some significant advantages in the treatment of neoplasm.

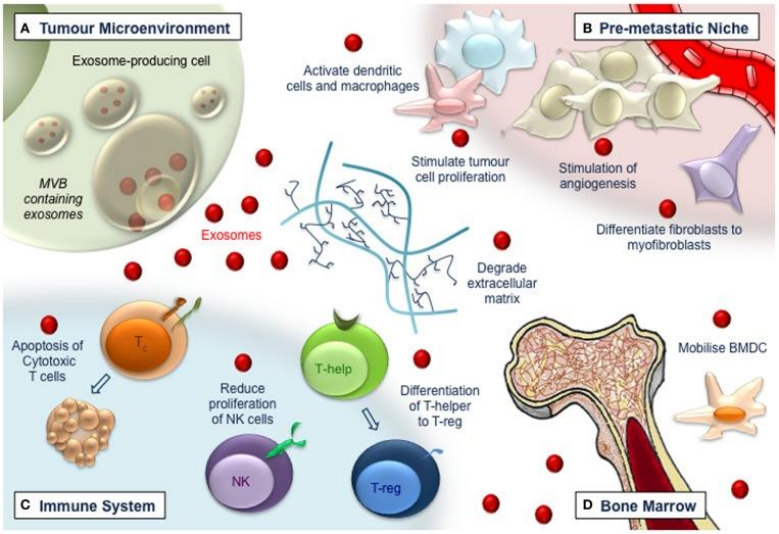

Figure 1. The role of extracellular vesicles in tumorigenesis (Tickner JA et al, 2014)

Unlike soluble factors secreted by cells, EVs bring functional molecules, which serve as intra- and inter-cellular communicators, locally and systemically (Togliatto et al, 2016). EVs can promote tumor growth and metastasis even by inducing angiogenesis (Valadi et al, 2007; Grange et al, 2011; Sceneay et al, 2013; Gacche et al, 2013; Tickner et al, 2014; Penfornis et al, 2016; Giusti et al, 2016;). This event has been extensively documented in tumor cell-derived EVs (Kharaziha et al, 2012). However, ECs themselves can release EVs in response to angiogenic stimuli (Lombardo et al, 2016), thus also contributing to the angiogenic activity of growing microvessels.

The canonical Wnt/β-Catenin pathway

The Wnt signaling pathways, named for its ligands Drosophila wingless (wg) and the mouse homolog Int-1 (Wnt-1) (Baker, 1988), are a group of signal transduction pathways which play a fundamental role in the cell fate specification during early embryonic development, proliferation, body axis patterning, survival, apoptosis, and in tissue homeostasis in adults (Croce et al, 2008). Aberrant activation of this pathway can cause uncontrolled cell growth and cell malignant transformation (Logan et al, 2004; Clevers, 2006).

Wnt proteins consist of a family of secreted glycoproteins ~40 kDa in size, characterized by several conserved cysteine residues. There are 19 human WNT genes, several of which encode additional, alternatively spliced isoforms (Miller, 2002).

Wnt signaling pathways can be activated upon binding of Wnt ligands to their cell surface receptor, Frizzled (FZD), and the LDL receptor-related proteins-5 or -6 (Kiewisz et al, 2015; Song et al, 2015; Bastakoty et al, 2016; Yang et al, 2016). As a consequence, the cytoplasmic protein Disheveled (Dvl) is phosphorylated and drives the detachment of β-catenin from the "β-Catenin destruction complex" and beta-catenin stabilization. This complex consists of a number of members including the adenomatous polyposis coli (APC), Axin, the glycogen synthase kinase 3 β (GSK3β) and the casein kinase 1α (CK1) (Kiewisz et al, 2015; Song et al, 2015; Bastakoty et al, 2016; Yang et al, 2016). Stabilized β-catenin translocates into the nucleus where it forms a β-catenin-T-cell

factor/lymphoid enhancer factor (TCF/LEF) transcriptional complex and induces the transcription of some of its downstream genes, such as c-myc and cyclin D1. In the absence of Wnt, cytoplasmic β-catenin is phosphorylated by activated GSK3β and undergoes proteasomal degradation (Kiewisz et al, 2015; Song et al, 2015; Bastakoty et al, 2016; Yang et al, 2016) (Figure 2).

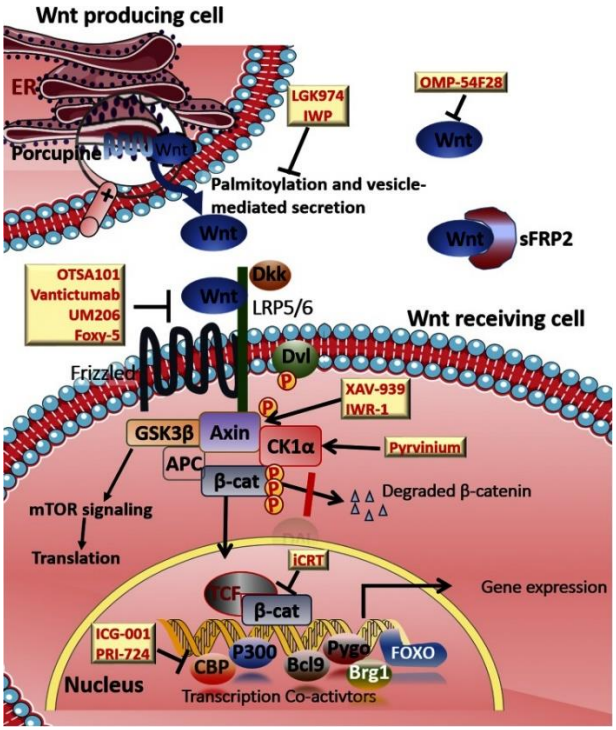

Figure 2. Simplified model of the canonical Wnt pathway and inhibitors (Bastakoty et al, 2016)

Several studies have described the Wnt-β-catenin pathway as a crucial regulator of EC fate during embryonic development and tumor angiogenesis (Miki et al, 2011; Hoffmeyer et al, 2012; Sun et al, 2013; Zhang et al, 2015; Ghahhari et al, 2015; Lin et al, 2017). Unlike in normal mature cells, the abnormal activation of the Wnt/β-catenin signal has been shown to occurs during cancer development (Hoffmeyer et al, 2012; Ghahhari et al, 2015; Kiewisz et al, 2015; Clevers et al, 2015; Liu et al, 2016).

miRs and Wnt/β-catenin pathway

Recent evidence suggest that newly discovered miRs, small non-coding RNA molecules, are important molecular regulators of pathways activated by tumor growth, including the Wnt/β-catenin pathway (Sun et al, 2013). This therefore, adds complexity in the regulation of diverse pathologic processes (Xu et Mo, 2012; Ghahhari et al, 2015; Chiurillo et al, 2015).

miRs are involved in the modulation of many biological processes by base pairing, usually imperfectly, to the 3′ untranslated region (UTR) of a target mRNA, resulting in posttranscriptional inhibition, and sometimes mRNA cleavage (Djuranovic et al, 2011). Because of this unique feature, a single miR can have multiple targets. Generally, many of these targets are involved in various signaling pathways so that their impact on gene expression can be significantly amplified. The miR function acting as oncogene or tumor suppressor in human neoplasms, is largely context-dependent or target-dependent (Xu et Mo, 2012). For example miR-203, which targets a cohort of pro-metastatic genes and growth factors, is sufficient to repress prostate carcinoma by inhibiting cell proliferation, migration and invasiveness (Saini et al, 2011; Viticchie et al, 2011; Bao et al, 2011; Boll et al, 2013). On the contrary, oncogenic miRs, such as miR-21 and miR-221/222, frequently overexpressed in a variety of cancers, can potentially induce cellular proliferation, migration, and invasiveness by targeting anti-oncogenic genes (Bao et al, 2011).

The canonical Wnt/β-catenin signaling is under multiple levels of control and various Wnt pathway components are frequently disrupted in human neoplasms either through genetic or epigenetic alterations (Huang et al, 2010). miRs can modulate β-catenin–dependent transcription in several ways, including direct inhibition of β-catenin mRNA expression or indirect inhibition of negative or positive regulators of β-catenin activity (Huang et al, 2010).

miRs, such as miR-200a, miR-320, miR-1862, miR-483-3p and miR-214, act as negative regulators to Wnt/β-catenin activity by directly targeting β-catenin, or other positive Wnt/β-catenin signaling pathway regulators of (miR-143, miR-375, miR-126, miR-145, miR-34a, miR-122, miR-

21, miR-8 and miR-218). miR let-7e and miR-126 negatively regulate Wnt/β-catenin signaling by enhancing GSK-3β activity resulting in reduction of β-catenin activity (Figure 3) (Sun et al, 2013).

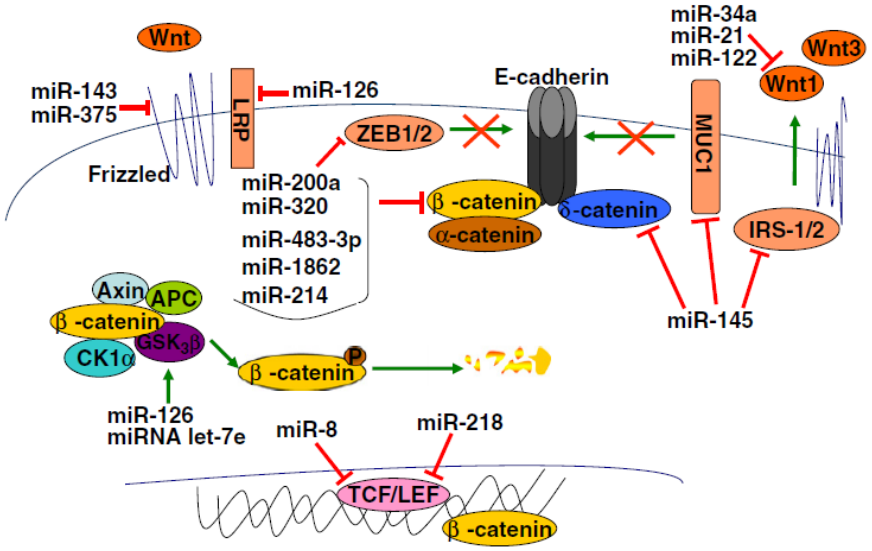

Figure 3. miRs acting upstream to Wnt/β-catenin signaling pathway (Sun et al, 2013)

miRs can also act as positive regulators of the Wnt/β-catenin signaling pathway: miR-290, miR-335-5p, miR-30a-5p, miR-31, miR-374a, miR-410 and miR-433 up-regulate Wnt/β-catenin signaling by targeting Wnt antagonists, including DKK, PRDM, WIF-1, sFRP. miR-27, miR-135a/b, miR-106b, miR-155, miR-315, let-7f miR and miR-26a activate the Wnt/β-catenin signaling by targeting genes such as APC, Axin, GSK3β and CK1α, which contribute to the formation of the "destruction complex". miR-499 can increase β-catenin activity acting on Dvl. Lastly, miR-17-5p, miR-130a, miR-141, miR-499 and miR-92b positively regulate Wnt/β-catenin signaling by targeting inhibitors of the β-catenin/TCF/LEF complex, such as P130, RUNX-3, NLK and SOX (Figure 4) (Sun et al, 2013).

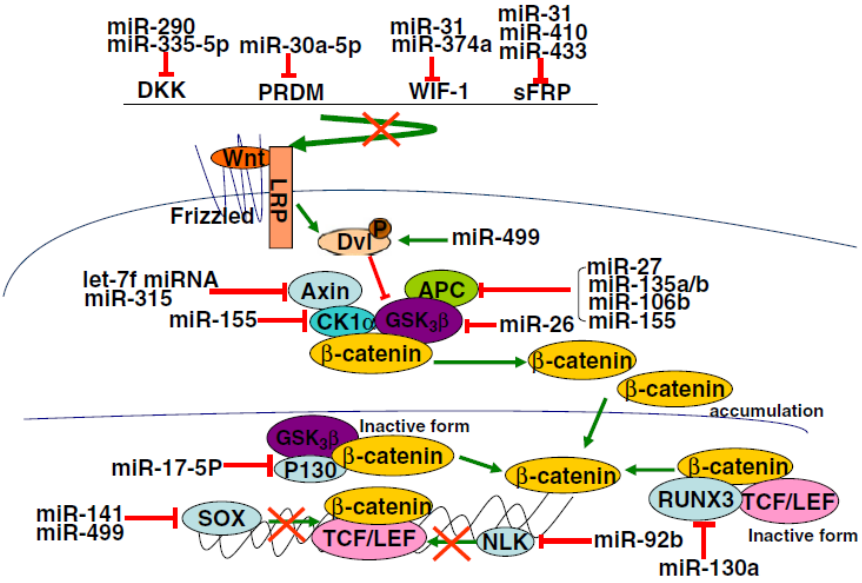

Figure 4. miRs acting as positive regulators of the Wnt/β-catenin signaling pathway (Sun et al, 2013).

AIM OF THE STUDY

We have recently provided evidence that EC-derived EVs mediate the transfer of activated proteins and in inflammatory sites containing IL-3, which, in turn, boost wound healing (Lombardo et al, 2016). These observations have led us to hypothesize that the release of IL-3 by TECs may also support the establishment of a favorable milieu via EVs. In this study, we have therefore decided to investigate the proangiogenic action of TEC-derived EVs and the impact of an anti-IL-3R-alpha blocking antibody, which is currently under investigation in acute myeloid leukemia patients (He SZ et al, 2015), on the proangiogenic effect of EVs released from TECs. Particular attention has been devoted to miR-EV cargo.

MATERIALS AND METHODS

Cell culture

Human breast-derived TECs were isolated and grown as previously described (Dentelli P et al, 2011; Bussolati B et al, 2003; Grange C et al, 2006). In selected experiments, starved TECs were cultured (24h) in the presence of EVs, anti-IL-3R-EVs or EVs that had either been depleted or enriched with (7×10^3 EVs/target cell) (Lombardo G et al, 2016). Untreated TECs served as controls. A Limulus amebocyte assay (concentration <0.1 ng/ml) (Charles River Laboratories, Inc., Wilmington, MA, USA) was used to test possible contamination. All experiments were performed in accordance with European Guidelines and policies and approved by the Ethical Committee of the University of Turin.

Isolation and quantification of TEC-derived EVs

TECs were cultured in EBM, without FBS, for 24h either with or without the anti-IL-3Rα neutralizing antibody in order to collect EVs from supernatants. After being centrifuged at 3000 g for 30 min to remove debris, cell-free supernatants were submitted to differential ultracentrifugation at 10 000 and 100 000g (Beckman Coulter Optima L-90K ultracentrifuge; Beckman Coulter, Fullerton, CA, USA) for 3h at 4°C. EVs were either used fresh or stored (-80°C) after re-suspension in EBM supplied with 1% DMSO (Deregibus MC et al, 2007; Togliatto et al, 2016). Frozen EVs were washed and pelleted by 100k g ultracentrifugation to remove DMSO before experiments. No differences in biological activity between fresh and stored EVs were observed. EV protein content was quantified using the Bradford method (Bio-Rad, Hercules, CA, USA). Possible contamination was tested for using a Limulus amebocyte assay (concentration <0.1 ng/ml) (Charles River Laboratories, Inc., Wilmington, MA, USA). EV size distribution analyses were performed using a NanoSight LM10 (NanoSight Ltd, Minton Park UK). The particles in the samples were illuminated using a laser light source and the scattered light was captured by camera and analyzed using Nanoparticle Tracking Analysis (NTA). NTA automatically tracked and sized particles according to

Brownian motion and the diffusion coefficient (Dt) (Gallo S et al, 2016). Results were displayed as a frequency size distribution graph and outputted to a spreadsheet. EVs were also collected from TECs subjected to loss- or gain-of-function experiments, as described below

EV internalization by TECs

The internalization of EVs into TECs was evaluated using confocal microscopy (LSM5-PASCAL; Zeiss, Oberkochen, Germany). A pool of EV particles was labeled with red fluorescent PKH26 dye (2 μl ml−1) for 30 min at 37 °C and EVs were then washed and ultracentrifuged at 100 000 g for 1 h at 4 °C. EV pellets were suspended in DMEM and added, at 7×10^3 EV/target cell concentration, to TECs for 3h in order to detect internalization (Lombardo G et al, 2016). The EV number was selected on the bases of our preliminary experiments performed by using EV number ranging from 5×10^3 to 1×10^4.

Cell Proliferation Assay

The proliferative activity of TECs, treated as indicated, was evaluated by Trypan blue at the end of each experiment, by a direct cell count (number±SD of cells per field, 10X magnification per sample). Each experiment was performed in triplicate and count was performed by three different operators. (Dentelli P et al, 2011; Togliatto G et al, 2016; Brizzi MF et al, 2004).

Western blot and co-immunoprecipitation analysis

TECs and TEC-derived EVs were lysed and protein concentrations obtained as previously described (Lombardo G et al, 2016; Dentelli P et al, 2009; Trombetta A et al, 2013). 50 μg protein for cells and 10 μg for EVs were processed as previously described (Brizzi MF et al, 2004). In selected experiments protein-A-Sepharose beads were used for co-immunoprecipitation experiments (Trombetta A et al, 2013). Protein levels were normalized to β-actin (Bruno S et al, 2017) or Histone-3 (H3). To evaluate β-catenin activity, cytoplasmic and nuclear extracts

(Trombetta A et al, 2013) from TECs, either treated or left untreated as indicated, were prepared as originally described (Sadowski HB et al, 1993). The presence of the anti-IL-3R antibody bound to TEC-derived EVs or retained in the EV-depleted CM, was also investigated by using an anti-mouse IgG. To this end EVs recovered from 100k g ultracentrifugation were directly subjected to Western blot analysis, while the supernatants were additionally ultracentrifuged for 24 h at 100k g to obtain EV-depleted CM. These CM were 50X concentrated and analyzed by Western blot.

RNA isolation and quantitative real-time PCR (qRT-PCR)

Total RNA was isolated from TECs, either treated or left untreated as indicated, using the TRIzol reagent (Invitrogen) and from indicated EVs using the mirVana RNA Isolation Kit (Ambion), according to manufacturer's instructions (Togliatto G et al, 2016). RNA was quantified spectrophotometrically (Nanodrop ND-1000, Wilmington, DE, USA) because intact 18S and 28S rRNAs were difficult to detect in the EVs. RNA, from cells and EVs, was then retrotranscribed using TaqMan microRNA RT kits, specific for miR-214-3p and miR-24-3p, and subjected to qRT-PCR using a TaqMan microRNA assay kit and the ABI PRISM 7700 sequence detection system (Applied Biosystems, Foster City, CA, USA). miR expression was normalized to the small nuclear RNA, RNU6B. In order to collect EVs, depleted of miR-24-3p or enriched in miR-214-3p, loss- and gain-of-function experiments were performed in TECs transfected for 48h with the antago-miR negative control, the antago-miR-24-3p, the pre-miR negative control or pre-miR-214-3p oligonucleotides (Applied Biosystem), according to manufacturer’s instructions (Lombardo et al, 2016; Gallo S et al, 2016).

miR Screening

TEC-derived EVs, anti-IL-3R-EVs, antago-miR-24-3p-EVs and pre-miR-214-3p-EVs (triplicate of 3 different preparations per sample) were analyzed for their miR content by quantitative real time (qRT) PCR using the Applied Biosystems TaqManH MicroRNA Assay

Human Panel Early Access kit (Life Technologies). The expression profile of 375 human mature miRs was examined via sequential steps of reverse transcription (Megaplex RT Pools; Life Technologies) using an Applied Biosystems 7900H qRT-PCR instrument, as previously described. Briefly, single stranded cDNA was generated from a total RNA sample (80 ng), obtained as above, by reverse transcription using a mixture of looped primers (Megaplex RT kit, Life Technologies) according to manufacturer's instructions. The pre-amplification reaction for each sample was performed using a TaqMan® PreAmp Master Mix 2X (Life Technologies) mixed with specific Megaplex™ PreAmp Primers (10X) (Life Technologies). Pre-amplified products were then diluted, loaded into the TaqMan MicroRNA Array and qRT-PCR experiments were performed. Raw Ct values were calculated using the SDS software version 2.3. A comparison of miR expression was conducted using the Expression Suite software (Life Technologies). Fold change in miR expression, across all samples, was calculated as 2-ΔΔCt using basal EVs as control and by normalizing the data using global normalization (Mestdagh P et al, 2009). The expression of of interest in the analysis was confirmed using the TaqMan microRNA specific assay kit (Applied Biosystems, Foster City, CA, USA), as described below.

Tube-like structure formation (*in-vitro* angiogenesis assay)

24-well-plates were coated with growth factor-reduced Matrigel matrix to analyze tube-like structure formation in TECs that were either treated with EVs, anti-IL-3R-EVs (7×10^3 EV/target cell which was found effective in preliminary experiments performed with different EV numbers ranging from 5×10^3 to 1×10^4) or left untreated (Cavallari C et al, 2017). After 24h, the number of tube-like structures formed was evaluated by three different operators (each experiment was performed in triplicate), counting 10 fields at 10X magnification, using a phase-contrast microscope (Leica DMIL, Wetzlar, Germany).

Study approval

Animal studies were conducted in accordance with the Italian National Institute of Health Guide for the Care and Use of Laboratory Animals (protocol no: 944/2015-PR). Mice were housed according to the Federation of European Laboratory Animal Science Association Guidelines and the Ethical Committee of the University of Turin. All experiments were performed in accordance with relevant guidelines and regulations.

***In-vivo* angiogenesis assay**

In order to evaluate the in-vivo angiogenic potential of TEC-derived EVs, SCID mice (Charles River Laboratories Italia Srl, Calco, LC, Italy) (four mice for each experimental group) were injected s.c. into the flank with a growth factor-reduced Matrigel matrix containing 1×10^6 TECs and 1×10^5/cell of different EVs or saline. The number of EVs was selected from preliminary results obtained by using 0.5×10^5/cell, 1×10^5/cell, and 2×10^5/cell (data not shown). Since no differences were detected between 1×10^5/cell and 2×10^5/cell the lower doses was used (data not shown). Matrigel plugs were removed and processed on day 7 after injection. In order to evaluate the in-vivo ability of EVs to induce vessel regression, either TEC-derived EVs or anti-IL-3R-EVs (1×10^5/injected cell), re-suspended in 20 µl of saline, were directly injected into the Matrigel plugs of SCID mice (four mice for each experimental group) on days 3 and 7 after TEC implantation (1×10^6 cells). An equal volume of saline was used in control mice. Matrigel plugs were removed and processed after 10 days. Recovered Matrigel plugs were fixed in 10% buffered formalin and embedded in paraffin for histological analyses. 5 µm thick paraffin Matrigel sections were routinely stained with Masson's Trichrome blue (Dako), according to manufacturer's instructions. The quantification of neoformed vessels was expressed as the number±SD of vessels per sample (20X magnification) (Dentelli et al, 2011). Only vessels possessing a patent lumen that contained red blood cells were considered for the study (Cavallari C et al, 2017).

Bioinformatic analyses

Ingenuity Pathway Analysis (IPA) Software (Ingenuity Systems, Qiagen, Redwood City, CA) was used to generate the interaction-network that correlated the miRs of interest and mRNAs. The DIANA-miRPath v3.0 database was interrogated by setting up KEGG annotations to select miR targeting pathways, according to their enrichment in p-values. Each miR and interaction dataset were entered and examined individually or together with other significant. The merging algorithm was considered where appropriate (Vlachos IS et al, 2015).

Statistical analysis

All data are reported as mean ±SD. The D'Agostino–Pearson test was used to test normality. Unpaired student *t*-tests were used to compare 2 experimental groups, while one-way ANOVA, followed by Tukey's multiple comparison test, to compare ≥ 3 experimental groups. The differences in the fold induction of protein contents were evaluated by densitometric analyses and reported as relative amount. For the *in vitro* experiments the minimum sample size to ensure 90% power between controls and experimental groups with a probability level of 0.05, two-tailed hypothesis, was three experiments performed in triplicate. For the *in vivo* experiments the minimum sample size to detect a 40% difference between controls and experimental groups, with 90% power and a probability level of 0.05 in a two-tailed hypothesis, was n=8 mice/group. P-values <0.05 were considered statistically significant (*p<0.05, **p<0.01, ***p<0.001). 3 independent and blinded investigators evaluated the *in vivo* outcomes. All statistical analyses were carried out using GraphPad Prism version 5.04 (Graph Pad Software, Inc, La Jolla, CA, USA).

REAGENTS	
Description:	**Purchased from:**
FBS (F6178), SDS (L3771), PIPES (P9291), Triton X-100 (T8787), Nonidet P-40 (74385), NaCl (S3014), NaF (S7920), Na_3OV_4 (S6508), $Na_4P_2O_7$ (P8010), $MgCl_2$ (M8266), KCl (P9541), HCl (258148), Na-azide (S2002), Hepes (H3375), Tris (T1503), EDTA (E6758), EGTA (E4378), ethanol (51976), aprotinin (A6279), pepstatin A (P5318), PMSF (P7626), DMSO (D8418), PKH26 dye (MINI26-1KT), leupeptin (L2884), penicillin-streptomycin (P4333), Trypsin (T4799), protein A–Sepharose beads (P3391)	Sigma-Aldrich (St Louis, MO, USA)
EBM Basal Medium (CC-3121)	Lonza Inc (Allendale, NJ, USA)
Protein molecular weight markers (161-0374), Acrylammide (161-0156), polyvinylidene difluoride (PVDF) membranes (162-0115), Bradford reagent (500-0205), ECL (170-5061)	Bio-Rad (Hercules, CA, USA)
Matrigel Basement Membrane Matrix Growth Factor Reduced (356231)	BD Bioscience Pharmingen (Franklin Lakes, NJ, USA)
Lipofectin® Reagent (18292-037), TRIZOL (15596018), RNU6B (001093), hsa-miR-214-3p (002306), hsa-miR-24-3p (000402), has-miR-24 Anti-miR™ miRNA Inhibitor (AM10737), hsa-miR-214 Pre-miR™ miRNA Precursor (PM12124), Opti-MEM (11058021)	Invitrogen™ (Life Technologies Carlsbad, CA, USA; Paisley, UK).
ANTIBODIES	
Description:	**Purchased from:**
anti-β actin (sc-47778), anti-cyclin D1 (sc-20044), anti-CD81 (sc166029)	S. Cruz Biotechnology (Heidelberg, Germany)
anti-GSK3 β (ab93926), anti-APC (ab40778), anti-phospho S33 + S37 β catenin (ab11350), anti-β catenin (ab16051), anti-c-myc (ab32072), anti-CD63 (ab134045), anti-histone-H3 (ab1791)	Abcam (Cambrige, UK)
Human IL-3 R alpha Antibody (Mouse) (MAB301)	R&D System Inc. (Minneapolis, MN, USA)
anti-rabbit IgG, HRP linked (4050-05) anti-mouse IgG, HRP linked (1031-05)	Southern Biotech (Birmingham, Alabama USA)
β-TrCP (D13F10) , Phospho-β-Catenin (Ser33/37) Antibody #2009	Cell Signaling (EuroClone**,** Milan, Italy)

RESULTS

EVs released by TECs subjected to IL-3 receptor blockade reduce TEC proliferation

It has been reported that ECs, when subjected to IL-3, release EVs which act as paracrine proangiogenic mediators (Lombardo et al, 2016). To investigate whether and how TEC-derived EVs induce proangiogenic cues and whether this effect may be prevented by interfering with IL-3-mediated signaling, EVs were recovered after treating TECs with an antibody against the IL-3 receptor alpha subunit (anti-IL-3R-EVs). Firstly, we investigated whether differences in EV release occurred. No differences in the number and size of EVs released were found and reported in Figure 5 and Figure 6.

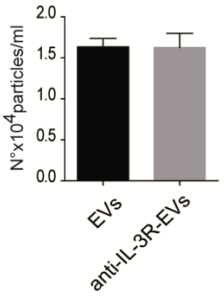

Figure 5. Number of EV particles (mean±SD) was calculated per ml. Data refer to EV-derived from untreated TECs (EVs) or anti-IL-3Rα blocking antibody-treated TECs (anti-IL-3R-EVs) (n=4, unpaired t-test).

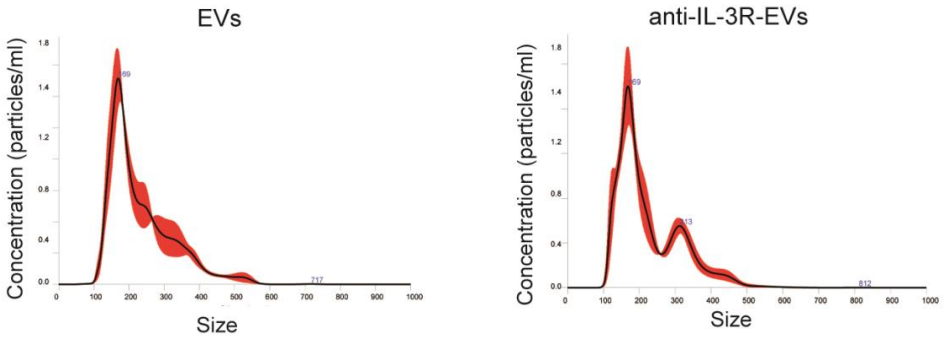

Figure 6. Representative images of NanoSight analyses performed on the 100 k fraction of TEC-derived EVs, showing a mean dimension, for both EVs, of 169 nm (n=3).

Moreover, we also analyzed exosome expression markers which are reported in Figure 7.

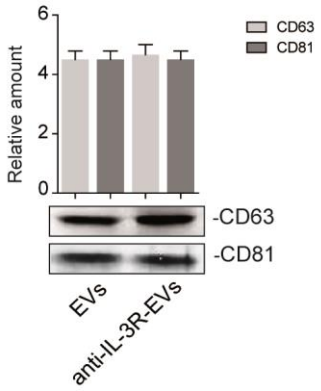

Figure 7. TEC-derived EVs were analyzed for CD63 and CD81 exosomal markers by Western blot analysis (n=4, unpaired t-test).

In order to evaluate whether EVs released under both experimental conditions could be internalized to act as paracrine mediators, EVs labeled with PKH26 dye were assayed for TEC internalization. As reported in Figure 8 both EVs and anti-IL-3R-EVs can be incorporated by TECs.

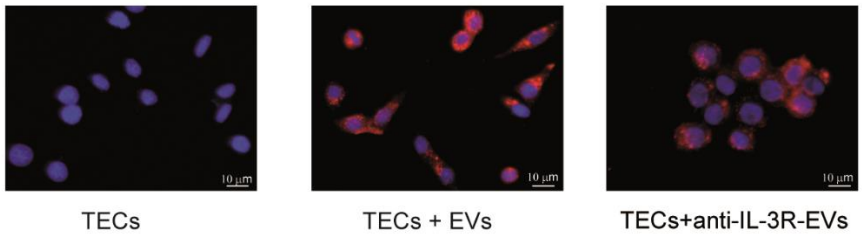

Figure 8. Representative confocal microscopy images of TECs, either untreated or treated for 3h with the indicated PKH26-labeled EVs, to evaluate EV up-take TECs. (n =4). Scale bars indicate 10 µm (40X magnification).

To exclude the possibility that the anti-IL-3R antibody bound to EVs could mediate the effects of anti-IL-3R-EVs, Western blot analysis was performed on anti-IL-3R EV pellet and anti-IL-3R-EV-depleted conditioned medium (CM). As shown in Figure 9a and Figure 9b we clearly demonstrated the presence of the anti-IL-3R antibody in the anti-IL-3R-EV-depleted CM, but not in the anti-IL-3R-EV pellets. EV-depleted CM and EV pellet from untreated TECs served as controls.

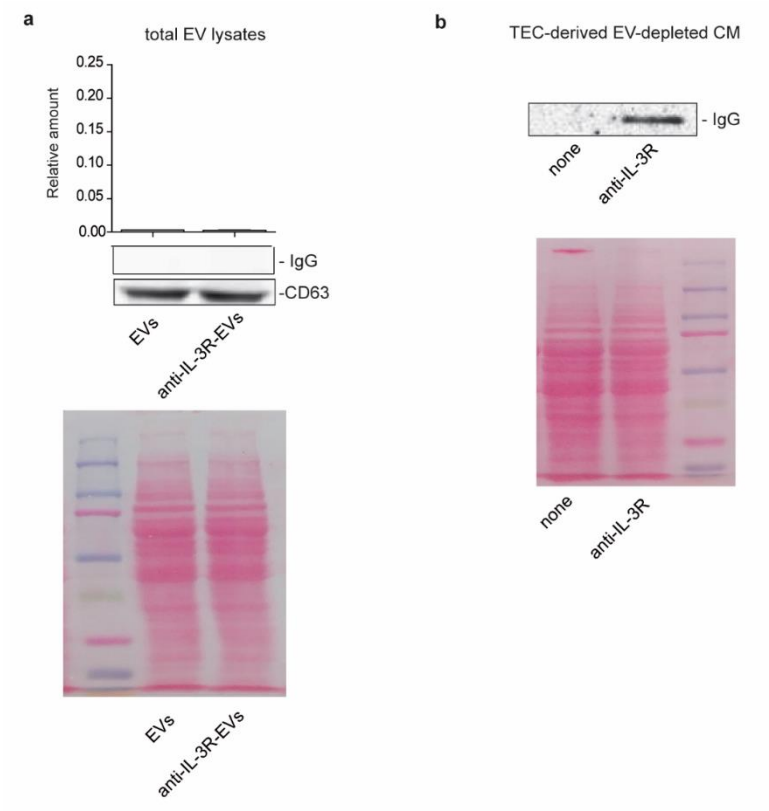

Figure 9. (a) EVs collected from untreated or anti-IL-3R-treated TECs were lysed and analyzed by western blot using an anti-mouse IgG antibody **(b)** The EV-derived CM obtained as described Materials and Methods were subjected to SDS-PAGE and analyzed as above described. Ponceau-stained membranes were used to demonstrate loaded proteins from each sample (EV-lysates and EV-depleted CM) (lower panels).

Functional studies were also performed by exploring the effect that EVs and anti-IL-3R-EVs had on TEC proliferation. Again, unstimulated TECs served as an internal control. To this end proliferation assay and cyclin D1 expression were evaluated. Both experimental approaches demonstrated that EVs promoted TEC proliferation (Figure 10), and that this effect was significantly reduced in TECs treated with anti-IL-3R-EVs.

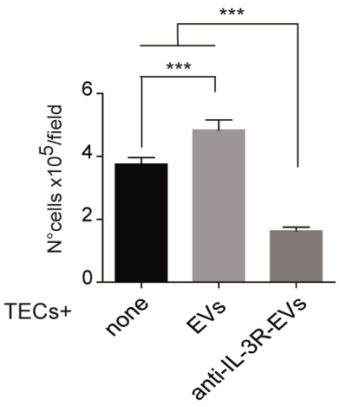

Figure 10. Cell proliferation assay was performed in TECs untreated (none) or treated for 24h with EVs or anti-IL-3R-EVs and reported as number of cells per field (mean±SD, 20X magnification) (n=5) (***p<0.001, none vs EVs; ***p<0.001, none and EVs vs anti-IL-3R-EVs, one-way ANOVA).

Low cyclin D1 levels were consistently detected in TECs that had been stimulated with anti-IL-3R-EVs (Figure 11). No differences in the number of apoptotic cells were found (data not shown).

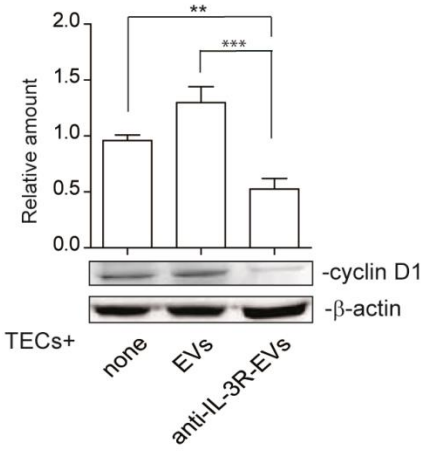

Figure 11. TECs, either alone or stimulated with EVs or anti-IL-3R-EVs, were lysed and analyzed for cyclin D1 content. Protein levels were normalized to β-actin content ***p<0.01*, none vs anti-IL-3R-EVs; ****p<0.001*, EVs vs anti-IL-3R-EVs, one-way ANOVA) (n=4).

anti-IL-3R-EVs prevent and impair the growth of tumor vessels

An *in-vitro* angiogenic assay was performed in order to evaluate whether anti-IL-3R-EVs interfere with TECs' ability to form neovessels. As shown in Figure 12 we demonstrated that treatment of TECs with anti-IL-3R-EVs was associated with reduced formation of tube-like structures.

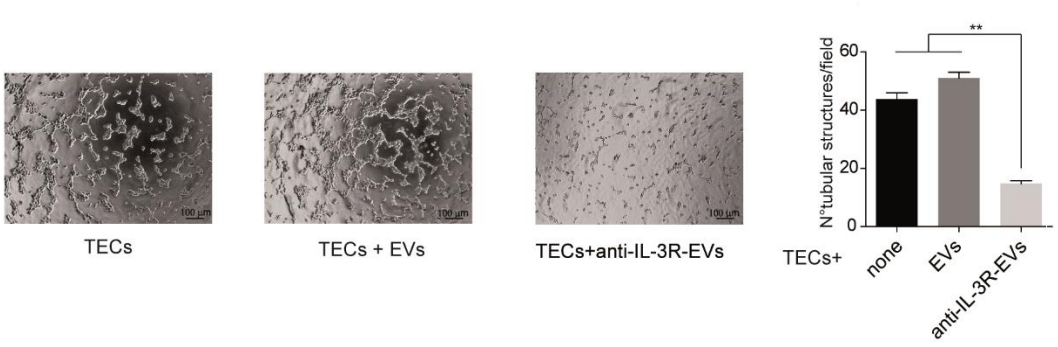

Figure 12. Representative photomicrographs of an *in-vitro* angiogenesis assay, showing tube-like structure formation by TECs, either untreated or treated with 7×10^3/cell EVs or anti-IL-3R-EVs. Data are reported in the histogram as number±SD of tubular structures per field (***p<0.01*, none and EVs vs anti-IL-3R-EVs, one-way ANOVA) (n=4, 10X magnification). Scale bars indicate 100 μm.

Two different *in-vivo* approaches were used to confirm the *in-vitro* effect. TECs, pre-incubated with EVs and anti-IL-3R-EVs, were included in Matrigel and injected subcutaneously into severe combined immunodeficient (SCID) mice. Seven days after implantation, plugs were recovered and analyzed for the presence of vessels. As shown by the reduced number of vessels observed in animals treated with anti-IL-3R-EVs, we were able to demonstrate that this treatment almost completely inhibited the angiogenetic capability of TECs (Figure 13).

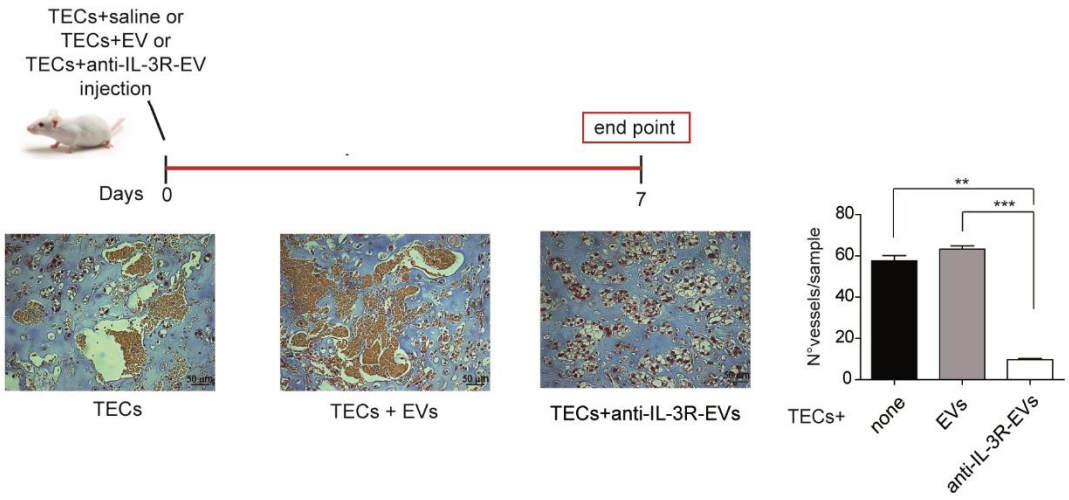

Figure 13. Representative images of an *in-vivo* angiogenesis assay, performed by injecting Matrigel matrices containing either 1×10^6 TECs and 1×10^5/cell of EVs or anti-IL-3R-EVs into the flank of SCID mice. Saline was the internal control. As shown by the timeline, plugs were recovered on day 7 after implantation. Data are reported in the histogram as number±SD of vessels per sample (***p<0.01*, none vs anti-IL-3R-EVs; ****p<0.001*, EVs vs anti-IL-3R-EVs, one-way ANOVA) (20X magnification). Scale bars indicate 50 μm.

In order to evaluate whether anti-IL-3R-EVs could also be exploited as a therapeutic option, *in-vivo* experiments were performed by injecting Matrigel-containing TECs into SCID mice and by treating them with either EVs, anti-IL-3R-EVs or saline administered locally on days 3 and 7 after implantation. The plugs were recovered and analyzed on day 10. It was found that mice treated with anti-IL-3R-EVs failed to form organized vessels *in-vivo*, unlike saline- or EV-treated animals, as shown in Figure 14. These results indicate that anti-IL-3R-EVs are also active in preventing and impairing the growth of tumor neovessels during tumor growth.

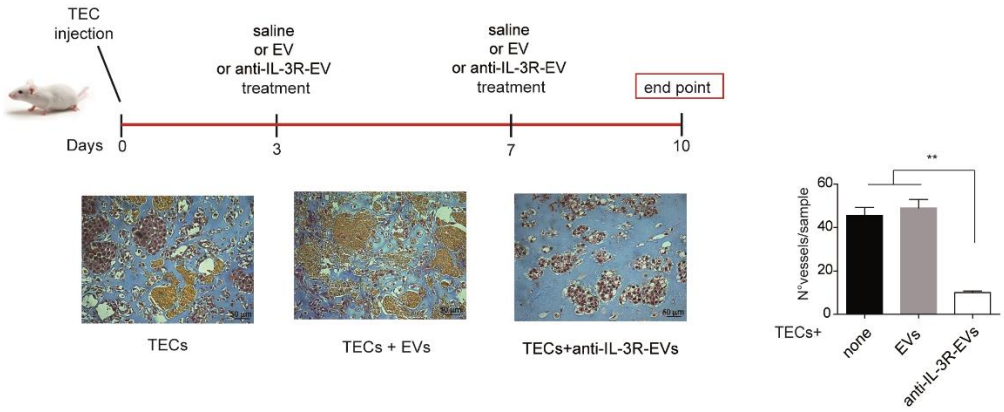

Figure 14. Representative images of an *in-vivo* angiogenesis assay to evaluate the ability of anti-IL-3R-EVs to impair the growth of tumor vessels. The timeline and the endpoint are indicated. Data are reported in the histogram as number±SD of vessels per sample (***p<0.01*, none and EVs vs anti-IL-3R-EVs, one-way ANOVA) (20X magnification). Scale bars indicate 50 μm.

anti-IL-3R-EV-mediated biological effects depend on their miR cargo variation

EV biological activity relies on the transfer into recipient cells of proteins, lipids and genetic material, including miRs (Deregibus et al, 2007; Camussi et al, 2010; Lee et al, 2012; Tickner et al, 2014; Penfornis et al, 2016; Togliatto et al, 2016). Anti-IL-3R-EV miR content was therefore compared to that of EVs in order to investigate the molecular mechanisms that account for *in-vivo* results. A complete panel of mature was screened. Figure 15a-b shows the distribution of that were up-upregulated and down-regulated in anti-IL-3R-EVs.

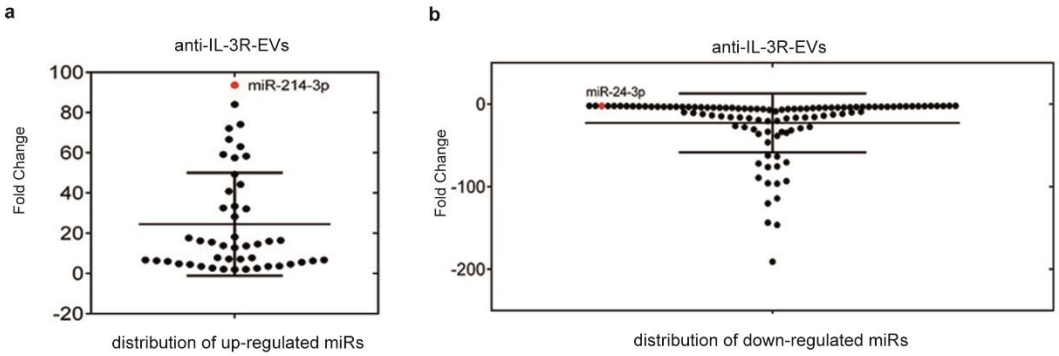

Figure 15. (a) Dot plot graph distribution of the 47 significant up-regulated miRs in anti-IL-3R-EVs, compared to EVs**.** Each dot represents the fold change value of each miR. Only miRs with fold change ≥ 2 are reported. miR-214-3p (red dot) was found as the most up-regulated miR in anti-IL-3R-EVs (fold change: 93.63± 4.52). **(b)** Dot plot graph distribution of the 107 significant down-regulated miRs in anti-IL-3R-EVs, compared to EVs. miRs with fold change ≤ 2 are reported. miR-24-3p (red dot) was found to be downregulated (fold change: -2.17± 0.08).

While the complete miR fold changes is reported in Tables 2 and 3.

miR	*fold change*	*miR*	*fold change*
hsa-miR-489	-190.73 ± 0.01	hsa-miR-518d	-5.76 ± 0.20
hsa-miR-384	-146.16 ± 0.01	hsa-miR-509-5p	-5.62 ± 0.21
hsa-miR-372	-143.51 ± 0.01	hsa-miR-590-5p	-5.38 ± 0.03
hsa-miR-598	-120.32 ± 0.01	hsa-miR-146a	-5.36 ± 0.03
hsa-miR-101	-114.12 ± 0.01	hsa-miR-16	-5.30 ± 0.13
hsa-miR-200a	-96.28 ± 0.00	hsa-miR-454	-4.72 ± 0.10
hsa-miR-296-3p	-95.74 ± 0.01	hsa-miR-122	-4.43 ± 0.26
hsa-miR-579	-93.14 ± 0.02	hsa-miR-888	-4.41 ± 0.26
hsa-miR-204	-89.09 ± 0.00	hsa-miR-362-3p	-4.36 ± 0.26
hsa-miR-422a	-76.23 ± 0.00	hsa-miR-10a	-4.35 ± 0.04
hsa-miR-376b	-75.43 ± 0.02	hsa-miR-196b	-4.28 ± 0.26
hsa-miR-548d	-71.86 ± 0.02	hsa-miR-195	-4.23 ± 0.04
hsa-miR-520b	-70.47 ± 0.02	hsa-miR-548a	-4.12 ± 0.23
hsa-miR-520a#	-63.25 ± 0.02	hsa-miR-181a	-4.06 ± 0.12
hsa-miR-539	-62.24 ± 0.02	hsa-miR-183	-4.05 ± 0.03
hsa-miR-520e	-46.20 ± 0.03	hsa-miR-19a	-3.95 ± 0.13
hsa-miR-182	-38.40 ± 0.02	hsa-miR-886-3p	-3.76 ± 0.12
hsa-miR-876-3p	-36.05 ± 0.04	hsa-miR-618	-3.75 ± 0.14
hsa-miR-542-3p	-34.78 ± 0.04	hsa-miR-374	-3.68 ± 0.11
hsa-miR-340	-33.60 ± 0.04	hsa-miR-576-3p	-3.53 ± 0.23
hsa-miR-211	-33.53 ± 0.04	hsa-miR-199a-3p	-3.46 ± 0.31
hsa-miR-501	-31.70 ± 0.04	hsa-miR-139-5p	-3.37 ± 0.13
hsa-miR-654-3p	-30.50 ± 0.00	hsa-miR-100	-3.30 ± 0.00
hsa-miR-505	-29.18 ± 0.05	hsa-miR-361	-3.21 ± 0.01
hsa-miR-382	-27.88 ± 0.05	hsa-miR-449b	-3.20 ± 0.31
hsa-miR-518d-5p	-27.52 ± 0.05	hsa-miR-515-5p	-3.19 ± 0.13
hsa-miR-127	-26.38 ± 0.03	hsa-miR-103	-3.16 ± 0.03
hsa-miR-190	-20.54 ± 0.02	hsa-miR-148b	-3.15 ± 0.24
hsa-miR-220b	-20.21 ± 0.07	hsa-miR-186	-3.10 ± 0.12
hsa-miR-629	-19.34 ± 0.07	hsa-miR-375	-3.09 ± 0.32
hsa-miR-627	-17.26 ± 0.08	hsa-miR-130a	-3.05 ± 0.05
hsa-miR-32	-17.03 ± 0.08	hsa-miR-223	-3.03 ± 0.01
hsa-miR-381	-16.42 ± 0.08	hsa-miR-20a	-2.93 ± 0.11
hsa-miR-548d-5p	-16.11 ± 0.00	hsa-miR-191	-2.73 ± 0.19
hsa-miR-184	-16.02 ± 0.01	hsa-miR-221	-2.73 ± 0.04
hsa-miR-487b	-15.73 ± 0.01	hsa-miR-194	-2.70 ± 0.14
hsa-miR-22	-15.60 ± 0.09	hsa-miR-335	-2.70 ± 0.12
hsa-miR-548c-5p	-14.64 ± 0.09	hsa-miR-130b	-2.56 ± 0.09
hsa-miR-450b-5p	-13.92 ± 0.01	hsa-miR-320	-2.53 ± 0.25
hsa-miR-136	-13.39 ± 0.09	hsa-miR-452	-2.49 ± 0.03
hsa-miR-146b	-12.42 ± 0.09	hsa-miR-17	-2.33 ± 0.06
hsa-miR-135b	-11.80 ± 0.09	hsa-miR-30c	-2.29 ± 0.02
hsa-miR-133a	-11.72 ± 0.11	hsa-miR-106b	-2.22 ± 0.01
hsa-miR-142-3p	-10.63 ± 0.05	hsa-miR-24	-2.17 ± 0.08
hsa-miR-26b	-9.99 ± 0.08	hsa-miR-193b	-2.16 ± 0.24
hsa-miR-362	-9.76 ± 0.13	hsa-miR-28	-2.16 ± 0.38
hsa-miR-525-3p	-9.16 ± 0.14	hsa-miR-20b	-2.14 ± 0.04
hsa-miR-455-3p	-8.65 ± 0.02	hsa-miR-106a	-2.13 ± 0.12
hsa-miR-26a	-7.04 ± 0.15	hsa-miR-25	-2.12 ± 0.06
hsa-miR-215	-6.63 ± 0.18	hsa-miR-149	-2.08 ± 0.16
hsa-miR-95	-6.07 ± 0.20	hsa-miR-99a	-2.06 ± 0.00
hsa-miR-548c	-5.94 ± 0.20	hsa-miR-105	-2.02 ± 0.04
hsa-miR-126	-5.79 ± 0.12	hsa-miR-125b	-2.01 ± 0.12
hsa-miR-660	-5.76 ± 0.13		

Table 2. Significantly down-regulated miRs (fold change values ≤ -2 ±SD in anti-IL-3R-EVs normalized to EVs) are listed.

miR	*fold change*	
hsa-miR-29c	2.01	± 0.39
hsa-miR-500	2.11	± 0.36
hsa-miR-29b	2.17	± 0.88
hsa-miR-515-3p	2.60	± 0.26
hsa-miR-521	2.68	± 0.85
hsa-miR-193a-3p	3.53	± 0.47
hsa-miR-301b	3.59	± 0.65
hsa-miR-518e	3.70	± 0.72
hsa-miR-519d	4.49	± 0.21
hsa-miR-652	4.60	± 0.26
hsa-miR-410	4.81	± 0.28
hsa-miR-494	5.63	± 0.28
hsa-miR-542-5p	6.04	± 0.13
hsa-miR-519a	6.33	± 1.12
hsa-miR-625	6.34	± 1.39
hsa-miR-338-3p	6.71	± 0.73
hsa-miR-518b	6.74	± 1.09
hsa-miR-582-5p	7.15	± 1.21
hsa-miR-589	7.21	± 0.37
hsa-miR-485-3p	7.75	± 0.47
hsa-miR-296	7.85	± 1.55
hsa-miR-616	12.85	± 0.77
hsa-miR-411	13.67	± 0.76
hsa-miR-148a	13.87	± 2.18
hsa-miR-363	14.62	± 2.37
hsa-miR-576-5p	15.63	± 1.95
hsa-miR-503	16.00	± 2.23
hsa-miR-642	16.21	± 2.38
hsa-miR-450b-3p	16.42	± 1.23
hsa-miR-424	17.64	± 1.79
hsa-miR-9	18.18	± 2.13
hsa-miR-551b	28.24	± 2.61
hsa-miR-891a	32.15	± 3.32
hsa-miR-548b	32.60	± 2.49
hsa-miR-198	33.39	± 3.59
hsa-miR-208	40.90	± 4.71
hsa-miR-139-3p	44.25	± 4.02
hsa-miR-708	49.35	± 5.10
hsa-miR-582-3p	57.50	± 5.52
hsa-miR-373	58.33	± 1.43
hsa-miR-519e	59.18	± 4.33
hsa-miR-887	63.04	± 2.64
hsa-miR-532	66.62	± 3.65
hsa-miR-202	72.15	± 6.12
hsa-miR-492	74.11	± 3.35
hsa-miR-216a	84.05	± 6.81
hsa-miR-214	93.63	± 4.52

Table 3. Significantly up-regulated miRs (fold change values ≥ 2 ±SD in anti-IL-3R-EVs normalized to EVs) are listed

Software prediction analyses on modulated miRs in anti-IL-3R-EV cargo identified two that were differentially modulated and that shared a common pathway: the canonical Wnt-β-catenin pathway. These were found to act on different levels; miR-214-3p, which is up-regulated, directly targets β-catenin (Wang X et al, 2012), miR-24-3p, which is downregulated, targets two different "β-catenin destruction complex" genes, APC and GSK3β (TarBase v7.0) (Pillai MM et al, 2014). The expression of miR-24-3p and miR-214-3p in EVs and anti-IL-3R-EVs was validated by real-time PCR (Figure 16).

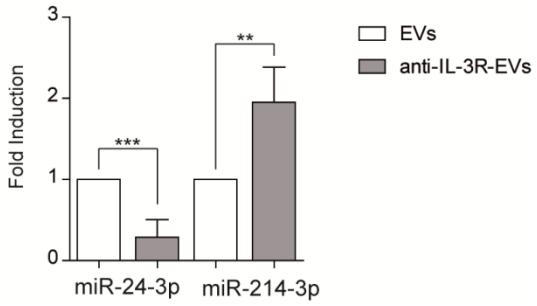

Figure 16. miR-24-3p and miR-214-3p expression was validated by qRT-PCR on EVs and anti-IL-3R-EVs and data normalized to RNU6B (n=4) (**p<0.01, EVs vs anti-IL-3R-EVs for miR-24-3p and miR-214-3p, unpaired t-test).

It was then decided to analyze the expression of phosphorylated and un-phosphorylated β-catenin in total cell lysates in TECs treated with EVs and anti-IL-3R-EVs in order to investigate the possibility that miR-24-3p and miR-214-3p, carried by anti-IL-3R-EVs, may interfere with the β-catenin signaling pathway. The results reported in Figure 17 clearly demonstrate an increase in phosphorylated, and a decrease in un-phosphorylated β-catenin content in TECs subjected to anti-IL-3R-EV treatment.

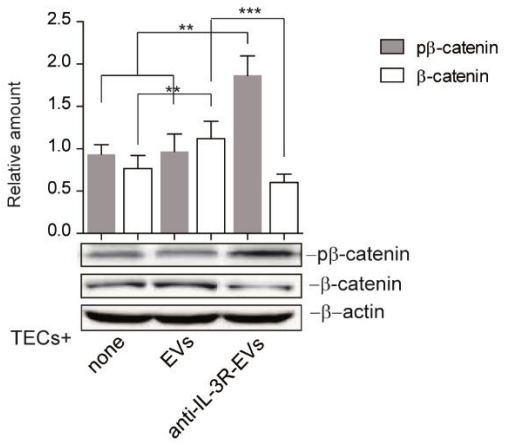

Figure 17. Total cell extracts from TECs, treated as indicated, were subjected to Western blot analysis to evaluate pβ-catenin and β-catenin content, normalized to β-actin (n=4) (***p<0.01* none and EVs vs anti-IL-3R-EVs for pβ-catenin; ***p<0.01* none vs EVs for β-catenin; ****p<0.001* EVs vs anti-IL-3R-EVs for β-catenin, one-way ANOVA).

To evaluate the possibility that changes in the expression of un-phosphorylated β-catenin in TECs treated with anti-IL-3R could occur, its expression was also analyzed. Figure 18 clearly demonstrates that in this experimental condition, the level of un-phosphorylated β-catenin did not change.

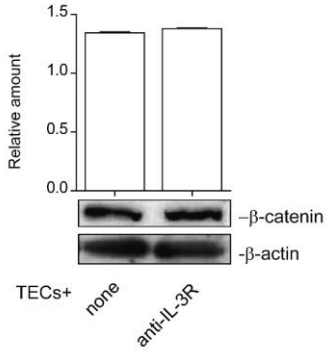

Figure 18. Cell extracts from untreated or anti-IL-3R-treated TECs were analyzed for β-catenin content, normalized to β-actin (n=3).

The canonical Wnt/*β*-Catenin pathway is targeted by anti-IL-3R-EVs

APC and GSK3β, known to be under the control of miR-24-3p, were evaluated to gain further insight into the anti-IL-3R-EV mechanism of action. As shown in Figure 19, both APC and GSK3β levels increased after anti-IL-3R-EV treatment.

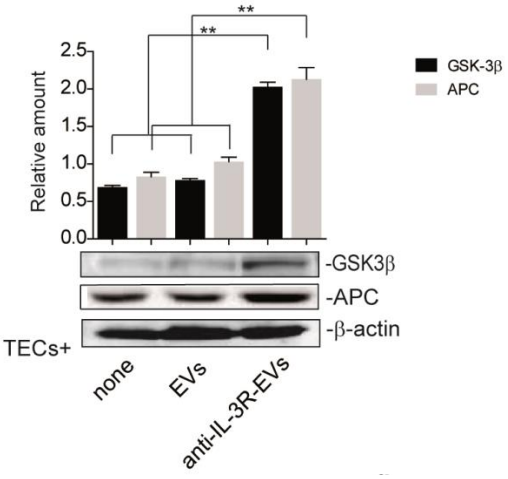

Figure 19. Cytoplasmic extracts from TECs, treated as indicated, were subjected to Western blot analysis to evaluate APC and GSK 3β content, normalized to β-actin (n=4) (**p<0.01, none and EVs vs anti-IL-3R-EVs, one-way ANOVA).

As for un-phosphorylated β-catenin also APC, GSK 3β and phosphorylated β-catenin level did not change in anti-IL-3R-treated TECs (Figure 20).

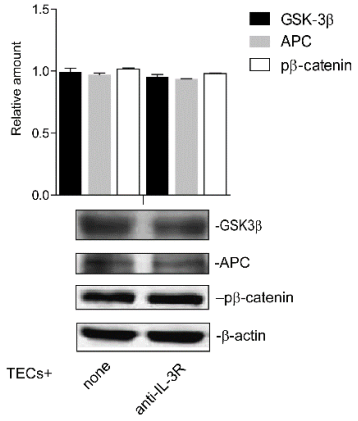

Figure 20. TECs treated as above were lysed and analyzed to evaluate GSK 3β, APC and pβ-catenin content, normalized to β-actin (n=3).

To exclude the possibility that EVs can be enriched and transfer these molecules EV protein content was analyze both in naïve and anti-IL-3R-EVs. As shown in Figure 21, APC and GSK3β were neither detected in naive nor in anti-IL-3R-EVs.

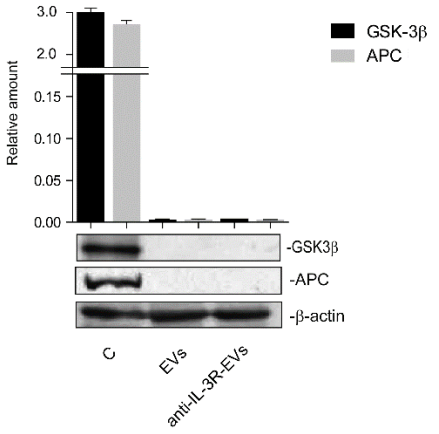

Figure 21. Total EV lysates were subjected to SDS-PAGE to evaluate GSK 3β and APC content, normalized to β-actin (n=3). Total cell lysate from untreated TECs was used as positive control (C).

Consistent with our hypothesis and data above reported β-catenin was strongly reduced in the nuclear fraction (Figure 22) of TECs treated with anti-IL-3R-EVs. These results are consistent with the increase in "β-catenin destruction complex" components.

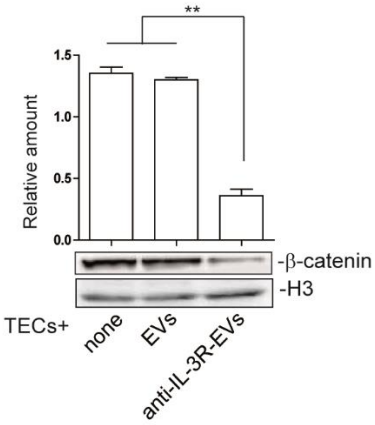

Figure 22. Nuclear extracts from TECs, treated as above, were analyzed for β-catenin content and normalized to H3 (n=3) (**p<0.01, none and EVs vs anti-IL-3R-EVs, one-way ANOVA).

This was further validated by immunoprecipitation experiments using an antibody against the beta-transducing repeats-containing proteins (β-TrCP), which act as the substrate recognition subunits for the SCF (Skp1–Cullin1–Fbox protein) $^{\beta\text{-TrCP}}$ E3 ubiquitin ligases (Fuchs SY et al, 2004). Indeed, a complex containing the phosphorylated β-catenin and β-TrCP was detected upon anti-IL-3R-EV treatment (Figure 23).

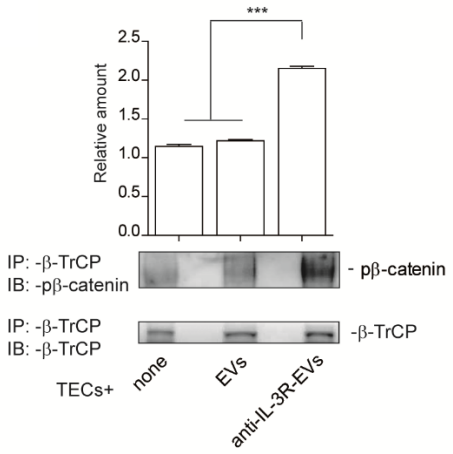

Figure 23. Cytoplasmic extracts from untreated or treated TECs, as indicated, were immunoprecipitated with anti-β-TrCP antibody, subjected to SDS-PAGE and immunoblotted with anti-pβ-catenin and anti-β-TrCP antibodies (***$p<0.001$, none and EVs vs anti-IL-3R-EVs, one-way ANOVA).

Since β-catenin content was reduced in the total lysates of anti-IL-3R-EV-treated TECs (Figure 17), it was decided to determine whether the enrichment of miR-214-3p in anti-IL-3R-EVs could exert a direct β-catenin expression effect. Gain-of-function experiments were therefore performed. To this purpose, TECs were transfected with pre-miR-214-3p and EVs were recovered (pre-miR-214-3p-EVs). Transfection efficacy was confirmed by real time PCR (rt-PCR) in both cells and EVs (Figure 24a-b).

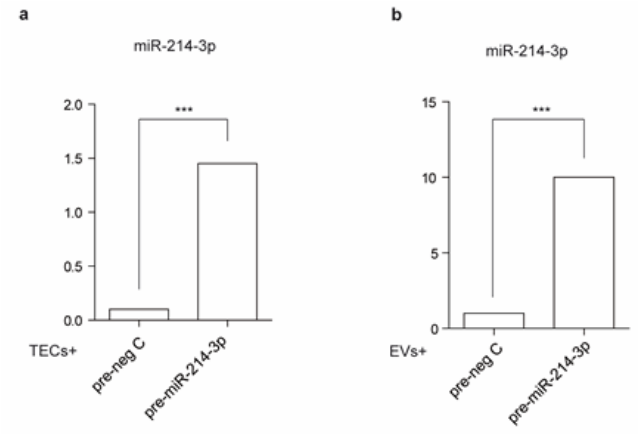

Figure 24. (a-b) Gain-of-function experiments were performed on TECs after 48h incubation with pre-miR-214-3p oligonucleotides. Pre-miR negative control (pre-neg c) oligonucleotides were used as control to evaluate the expression in both cells and EVs. miR-214-3p expression was evaluated by qRT-PCR either in transfected TECs (**a**) or in TEC-derived EVs (pre-miR-214-3p-EVs) **(b).** Data are normalized to RNU6B (n=5) (****p<0.001*, pre-miR-214-3p vs pre-miR-neg c in (**a**) and (**b**)).

The effects of pre-miR-214-3p on β-catenin expression were initially evaluated in transfected cells (Figure 25a) and then in TECs treated with pre-miR-214-3p-EVs (Figure 25b). As expected, β-catenin content was reduced both in transfected cells and in TECs stimulated with pre-miR-214-3p-EVs.

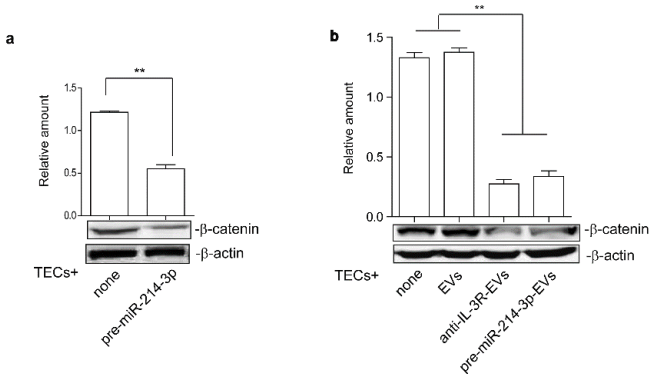

Figure 25. (a) TECs that over-express miR-214-3p were subjected to SDS-PAGE to evaluate β-catenin content, normalized to β-actin. Untransfected TECs were used as internal controls (none) (n=5) (**p<0.01, none vs pre-miR-214-3p, unpaired t-test). **(b)** Cell extracts from TECs, left untreated or treated with EVs, anti-IL-3R-EVs or EVs enriched in miR-214-3p, were analyzed for β-catenin content, normalized to β-actin (n=5) (**p<0.01, none and EVs vs anti-IL-3R-EVs and pre-miR-214-3p-EVs, one-way ANOVA).

The contribution of miR-24-3p to anti-IL-3R-EV-mediated action was then evaluated by performing loss-of-function experiments. TECs were transfected with antago-miR-24-3p and EVs (antago-miR-24-3p-EVs) were recovered. Antago-miR-24-3p depletion was confirmed by rt-PCR in cells and EVs (Figure 26a-b).

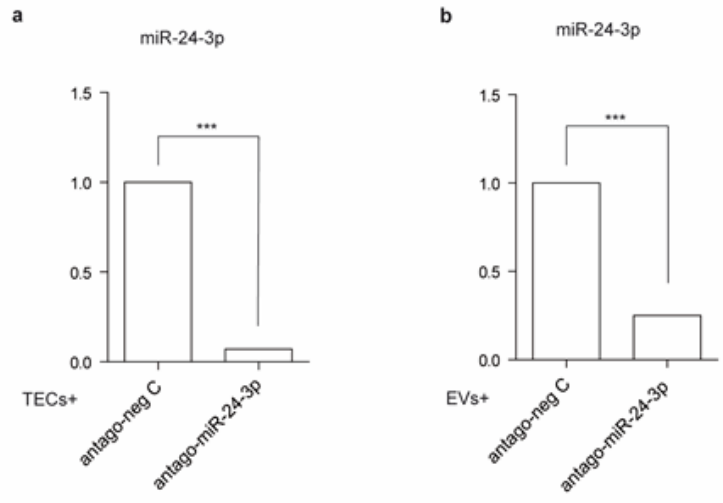

Figure 26. Loss-of-function experiments were performed on TECs after 48h incubation with antago-miR-24-3p. Antago-miR negative control (antago-neg c) was used as control. miR-24-3p expression was evaluated by qRT-PCR either in transfected TECs (**a**) or in TEC-derived EVs (antago-miR-24-3p-EVs) (**b**). Data are normalized to RNU6B (n=5) (****p<0.001*, antago-miR-24-3p vs antago-neg c in (**a**) and (**b**)).

As shown in Figure 27a-b, increased APC and GSK3β content was detected in both transfected cells and in antago-miR-24-3p-EV-treated TECs.

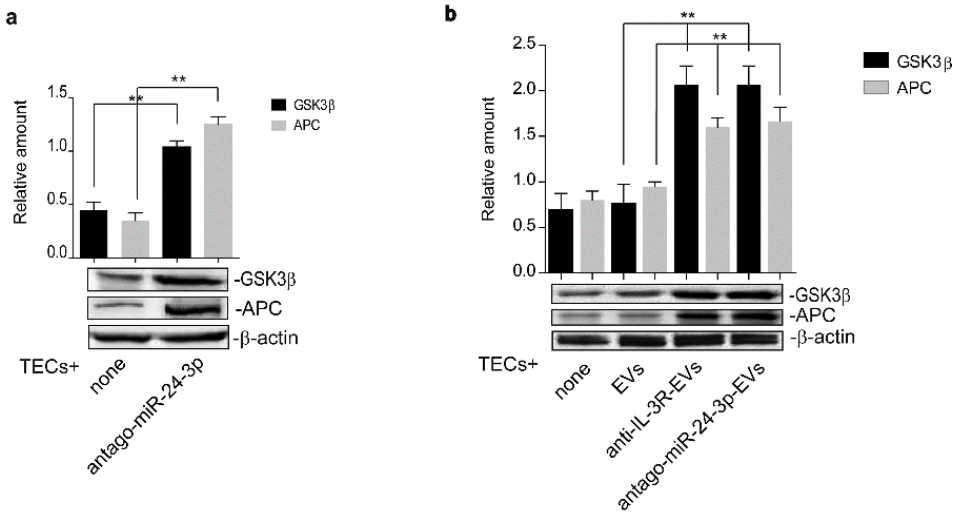

Figure 27. (a-b) Cytoplasmic extracts from TECs depleted of miR-24-3p (antago-miR-24-3p) **(a)** and from TECs treated with antago-miR-24-3p-EVs **(b)** were analyzed by Western blot for APC and GSK3β content (***p<0.01*, none vs antago-miR-24-3p in (c), unpaired *t*-test, and ***p<0.01*, EVs vs anti-IL-3R-EVs and antago-miR-24-3p-EVs in (d), one-way ANOVA).

Furthermore, increased levels of phosphorylated β-catenin and a decrease in unphosphorylated β-catenin were found (Figure 28a-b).

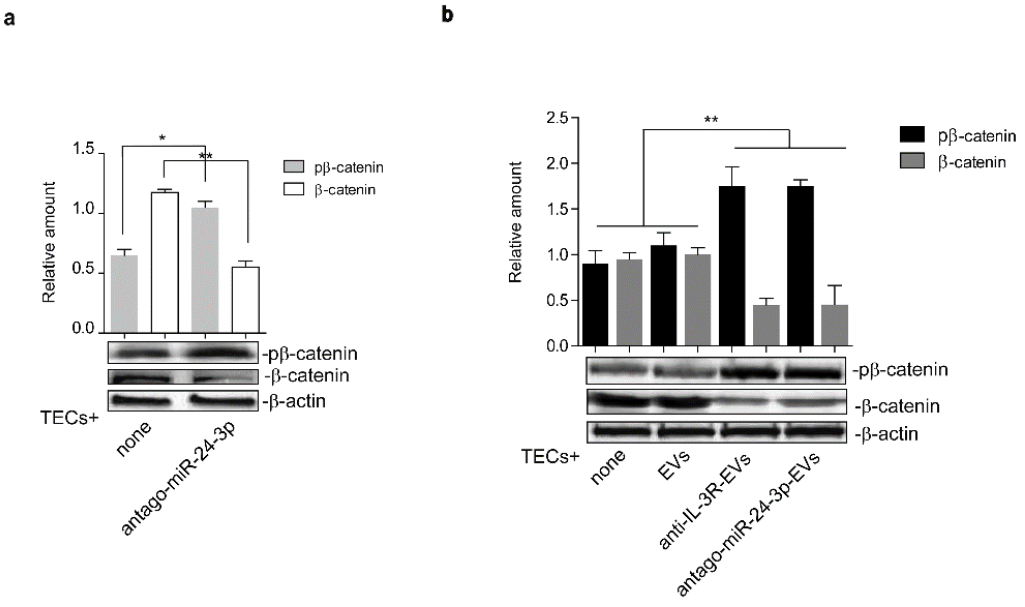

Figure 28. (a) Cell extracts from antago-miR-24-3p TECs and **(b)** from TECs, treated as above were analyzed for pβ-catenin and β-catenin content, normalized to β-actin (n=4) (**p<0.05*, for pβ-catenin and ***p<0.01*, for β-catenin, none vs antago-miR-24-3p in (a), unpaired *t*-test, and ***p<0.01*, none and EVs vs anti-IL-3R-EVs and antago-miR-24-3p-EVsin (b), one-way ANOVA).

To have additional information we have created an intersection of miR-24-3p and miR-214-3p using IPA Software. The integrated miR-24-3p and miR-214-3p interaction-network identified c-myc as one of their downstream nodes (Figure 29). The proto-oncogene c-Myc is a transcription factor well known for its role in the regulation of proliferation, growth, differentiation and survival of many cell types (Coller et al, 2000; Pelengaris et al, 2003). Deregulated c-Myc expression has been associated with cancer and vascular disorders (Baudino et al 2002; de Nigris et al, 2006; Napoli et al, 2006).

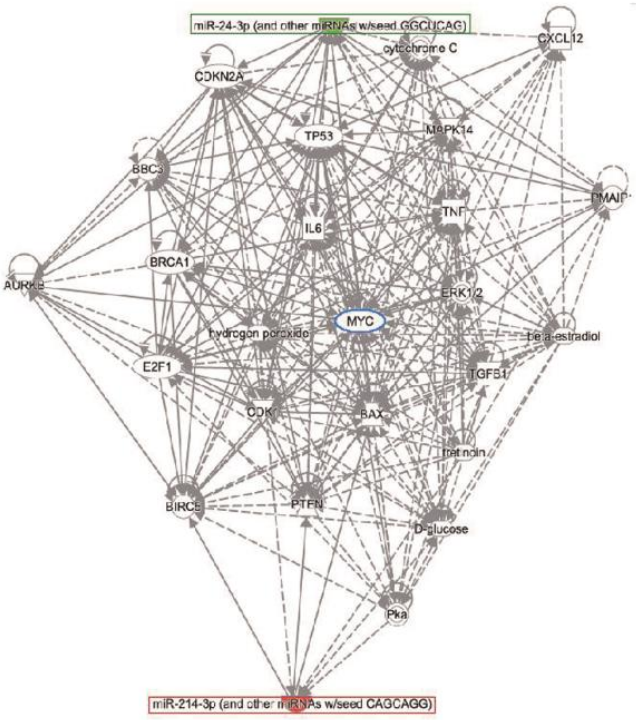

Figure 29. Network analysis between miR-24-3p/miR-214-3p and mRNA targets. Lines represent interactions between genes and miRs predicted by the IPA Software: indirect interactions (dotted lines), direct interactions (continuous lines).

c-myc expression was therefore analyzed on TECs treated with different EVs. As shown in Figure 30, anti-IL-3R-EVs, antago-miR-24-3p- and pre-miR-214-3p-EVs failed to induce c-myc expression, unlike EVs.

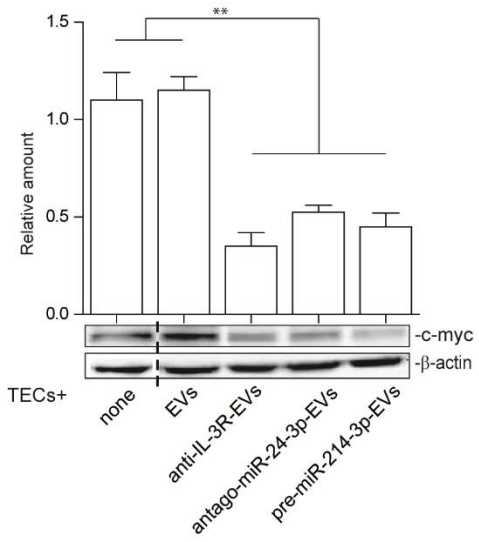

Figure 30. TECs treated as indicated were lysed and analyzed for c-myc content, normalized to β-actin content (n=5) (***p<0.01*, none and EVs vs anti-IL-3R-EVs, antago-miR-24-3p-EVs and pre-miR-214-3p-EVs, one-way ANOVA)

miR-214-3p and miR-24-3p are both involved in anti-IL-3R-EV-antiagiogenic effects

Functional studies were performed *in-vivo* to confirm our data. Differing EV sources were used to treat mice on day 3 and 7 after TEC injection. As shown in Figures 31a and 31b, both pre-miR-214-3p-EVs and antago-miR-24-3p-EVs strongly reduced TEC-derived vessels *in-vivo*. However, it was found that, unlike antago-miR-24-3p-EVs, pre-miR-214-3p-EVs were less effective in reducing vessel growth than anti-IL-3R-EVs, while the combo treatment completely recapitulated the anti-IL-3R-EV antiangiogenic effect.

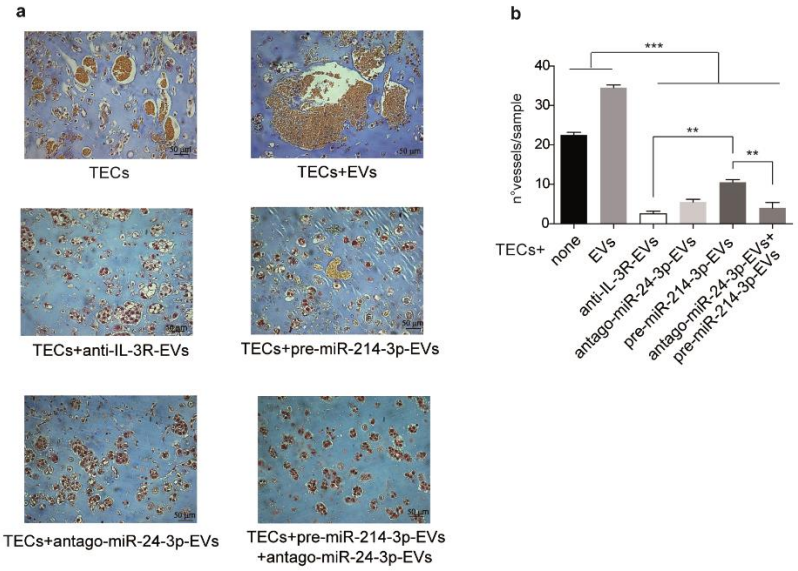

Figure 31. (a) Representative images of an in-vivo angiogenesis assay of TECs treated with antago-miR-24-3p-EVs and pre-miR-214-3p-EVs either alone or in combination. Untreated TECs and TECs treated with EVs and anti-IL-3R-EVs were also reported. (20X magnification). Scale bars indicate 50 μm **(b)** Data are reported in the histogram as number±SD of vessels per sample (***p<0.001, none and EVs vs others experimental conditions; **p<0.01, anti-IL-3R-EVs vs pre-miR-214-3p-EVs and pre-miR-214-3p-EVs vs antago-miR-24-3p-EVs +pre-miR-214-3p-EVs, one-way ANOVA)

In order to gain further insight into the mechanisms behind the differences in antago-miR-24-3p-EV and pre-miR-214-3p-EV *in-vivo* effects, miR cargo was analyzed and their fold change is reported in Supplementary Table 3 and 4.

miR	*fold change*		
hsa-miR-193b	0.17	±	0.29
hsa-miR-24	0.26	±	0.14
hsa-miR-342-3p	0.34	±	0.34
hsa-miR-320	0.61	±	0.12
hsa-miR-574-3p	0.63	±	0.39
hsa-miR-155	1.77	±	0.45
hsa-miR-886-5p	3.00	±	0.13
hsa-let-7e	3.42	±	0.06
hsa-miR-125a-5p	3.80	±	0.02
hsa-miR-214	594.33	±	3.01
hsa-miR-331	-12.51	±	2.88
hsa-miR-150	-7.62	±	0.84
hsa-miR-518d	-7.33	±	0.58
hsa-miR-365	-5.62	±	0.14
hsa-miR-17	-4.26	±	0.62
hsa-miR-16	-2.94	±	0.46
hsa-miR-19b	-1.95	±	0.44
hsa-miR-196b	-1.47	±	0.50
hsa-miR-191	-1.36	±	0.14
hsa-miR-484	-0.69	±	0.22
hsa-miR-222	-0.26	±	0.95

Table 6. Fold decrease/increase in miRs expressed by antago-miR-24-3p-EVs normalized to EVs are listed.

miR	*fold change*	
hsa-miR-574-3p	0.15	±0.20
hsa-miR-320	0.39	±0.21
hsa-miR-342-3p	0.44	±0.03
hsa-miR-155	1.17	±0.13
hsa-miR-125a-5p	2.00	±0.10
hsa-miR-214	3.80	±1.00
hsa-miR-106a	-26.78	±2.26
hsa-miR-24	-4.71	±0.76
hsa-miR-222	-4.26	±0.66
hsa-miR-484	-3.69	±0.24
hsa-miR-197	-1.79	±0.26
hsa-let-7e	-1.74	±0.44
hsa-miR-16	-1.67	±0.33
hsa-miR-193b	-1.62	±0.54
hsa-miR-191	-0.66	±0.03

Table 7. Fold increase/decrease in miRs expressed by pre-miR-214-3p-EVs normalized to EVs are listed.

Figure 32a-b shows how up-upregulated and down-regulated miRs distributed. It is worth noting to note that antago-miR-24-3p-EVs were found to be enriched in miR-214-3p (Figure 32a), while no changes in miR-24-3p content were detected in pre-miR-214-3p-EVs (Figure 32b).

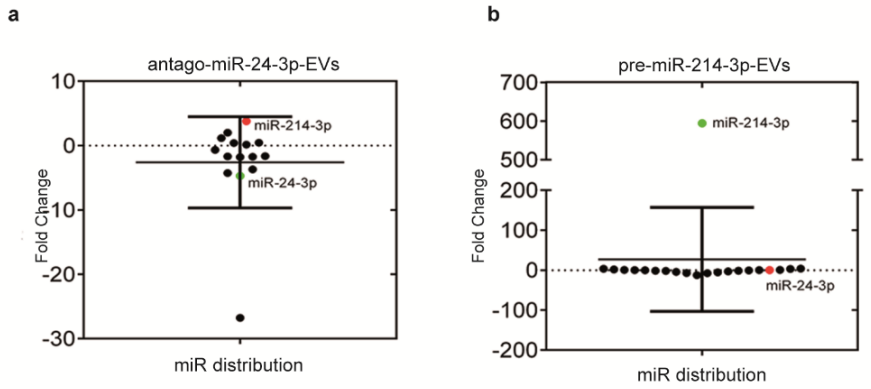

Figure 32. (a) Dot plot distribution graph of the 15 modulated miRs in antago-miR-24-3p-EVs compared to EVs. Dots represent fold change values for each miR. miR-214-3p (red dot) was found to be significantly up-regulated in antago-miR-24-3p EVs (fold change: 3.80± 1.00). **(b)** Dot plot distribution graph of the 21 modulated miRs in pre-miR-214-3p-EVs compared to EVs. miR-24-3p (red dot) was found to be almost unmodulated in pre-miR-214-3p-EVs (fold change: 0.26±0.14).

This finding is consistent with the reduced β-catenin expression reported in Figure 27a-b. A cross-match of miRs, carried by different EVs, was also performed. As shown in the Venn diagram (Figure 33), 4 miRs were downregulated in pre-miR-214-3p-EVs, antago-miR-24-3p-EVs and in anti-IL-3R-EVs.

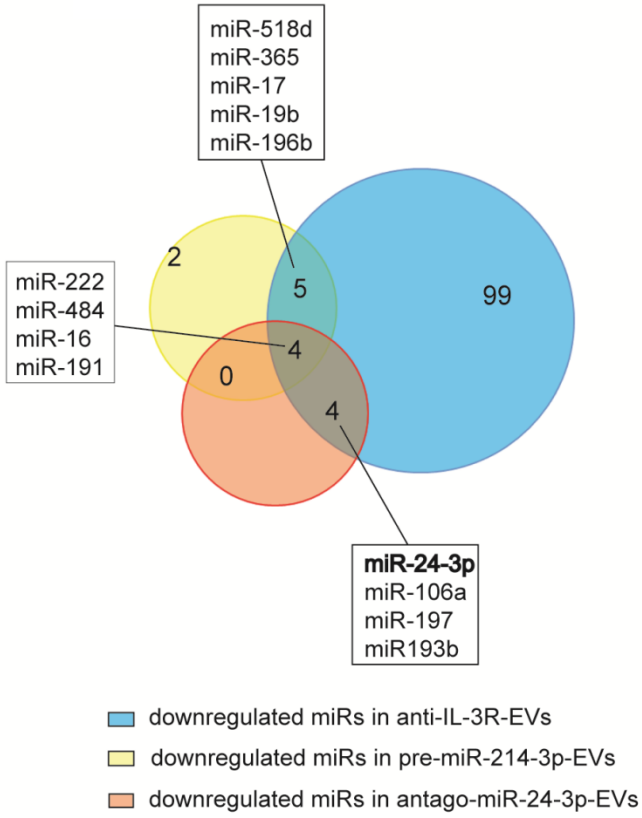

Figure 33. Venn diagram of downregulated miRs, identified in anti-IL-3R-EVs, antago-miR-24-3p EVs and pre-miR-214-3p EVs, are reported. The diagram shows an overlap of common miRs across different EVs

While the Venn diagram in Figure 34 shows the cross-match of up-regulated miRs shared by different EVs, only miR-214-3p was upregulated in all EVs. DIANA miR path software was therefore interrogated to identify the most relevant pathways which, along with Wnt-β-catenin, may contribute to the overlapping of the antiangiogenic effects detected in antago-miR-24-3p-, pre-miR214-3p-, and anti-IL-3R-EV treated animals (Figure 31b).

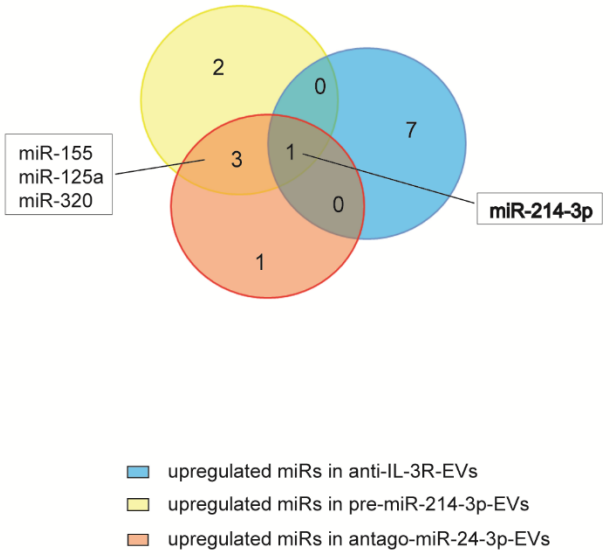

Figure 34. Venn diagram of upregulated miRs identified in anti-IL-3R-EVs, antago-miR-24-3p EVs and pre-miR-214-3p EVs. The diagram shows an overlap of common miRs among different EVs.

In particular, pathways correlating with down-regulated miRs shared by anti-IL-3R-EVs, pre-miR-214-3p-EVs and antago-miR-24-3p-EVs, or by anti-IL-3R-EVs and pre-miR-214-3p-EVs, or anti-IL-3R-EVs and antago-miR-24-3p-EVs were analyzed. As shown in Figure 35a and resumed in Figure 35b, miR-222-3p, miR-16-5p, miR-484, miR-17-5p, miR-106a-5p, miR-365b-5p, miR-196b-5p, miR-19b-3p, miR-197-3p, and miR-193b-3p significantly correlated with at least 2 of the following pathways: pathway in cancer, adherens junction, p53 signaling pathway, cell-cycle and ECM receptor interaction; whereas, miR-518d-5p and miR-191-5p did not. Of note, miR-16-5p, commonly shared by pre-miR-214-3p-EVs, antago-miR-24-3p-EVs, and anti-IL-3R-EVs significantly correlated with 4 miRs of the above pathways. Such significant correlation was also found for miR-17-5p (in pre-miR-214-3p-EVs) and miR-193b-3p (in antago-miR-24-3p-EVs).

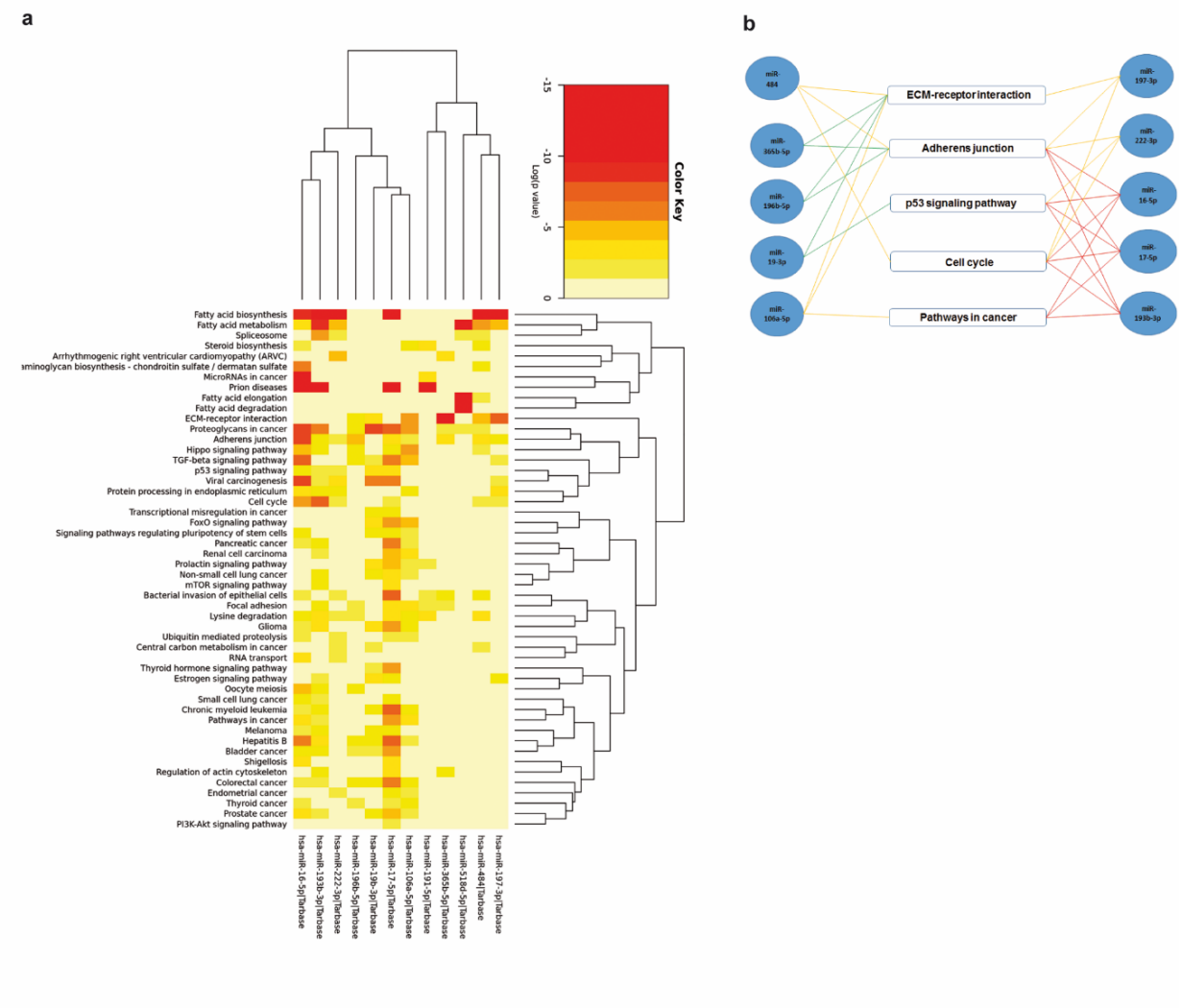

Figure 35. (a) Meta-analysis algorithm of the most significant pathways targeted by miR-222-3p, miR-16-5p, miR-484, miR-17-5p, miR-106a-5p, miR-365b-5p, miR-196b-5p, miR-19b-3p, miR-197-3p, miR-193b-3p, miR-518d-5p and miR-191-5p. Relevant correlation with the following pathways was found; cell cycle pathway (p-value=9,55-11), adherens junction (p-value=1.0-325), pathway in cancer (p-value=1.9-8), ECM-receptor interaction (p-value=1.0-325) and p53 signaling pathway (p-value=1.27-8). (Image from DIANA-miRpath software). Color notation identifies Log (p-value). **(b)** Representative scheme of DIANA miRpath analysis between miRs and correlated pathways. miRs were linked with pathways by lines of different colours. Red lines: miRs involved in 4 pathways; yellow lines: miRs involved in 3 pathways; green lines: miRs involved in 2 pathways

DISCUSSION

The microenvironment is a complex and dynamic tissue in tumor. The tumor and the surrounding microenvironment are closely related and interact constantly. Tumors can influence the microenvironment by releasing extracellular signals, promoting tumor angiogenesis and inducing peripheral immune tolerance, while the immune cells in the microenvironment can affect the growth and evolution of cancerous cells (Spano et al, 2012). A host of soluble factors have been widely found to modulate this environment. We have previously shown that IL-3 can promote EC proliferation and *in-vivo* angiogenesis (Dentelli et al, 1999). Moreover, it has been shown that signals emanated by IL-3, released by tumor infiltrating T-cells, promote *in-vivo* tumor expansion by increasing tumor neovascularization (Dentelli et al, 2005; Uberti et al, 2010).

However, intercellular crosstalk can also occur in the tumor microenvironment via direct cell-to-cell contact or via mediators that have secreted into the extracellular environment (Tickner et al, 2014). EVs have become recognized as an important part of cellular communication between cancer cells and cells within the tumor microenvironment (Grange et al, 2011; Gomes et al, 2013; Penfornis et al, 2016). Cancer cells actively interact with stromal cells through EVs. Data on invasive prostate cancer cell lines showed that cancer cells could not only activate fibroblasts in tumor stroma by secreting EVs, but also promote EV release from the activated fibroblasts to promote their own migration and invasiveness. EVs also contribute to the transformation of normal cells into cancer cells. As a matter of fact, studies on breast carcinoma and glioma cells showed that cancer cell-derived EVs transfer transglutaminase to both normal fibroblasts and epithelial cells and induce their transformation (Giusti et al, 2016). Similar to cancer cells, normal cells secrete EVs. Their function depends on the phenotype of the parent cells and the microenvironment. For example, EVs secreted by mesenchymal stem cells (MSCs) in breast cancers could support tumor growth in primary tumor models and inhibit metastasis formation in a metastatic model (Penfornis et al). As supported by these data, it is becoming evident that EV-mediated communication has a major influence on many aspects of tumor growth and progression (Tickner et al). Indeed, EVs

released from cancer cells, from stroma and vascular cells can promote tumor growth even by inducing tumor angiogenesis (Valadi et al, 2007; Sceneay et al, 2013; Gacche et al, 2013; Penfornis et al, 2016).

TECs diverge from their normal counterpart at the molecular and functional level (Dentelli et al, 2011). In fact, TECs show rapid turnover and express embryonic gene and vessel growth regulating molecules (Dentelli et al, 2011). Moreover, TECs derived from differing tissues, including breast and kidney tumors, produce IL-3 and are dependent on IL-3 for their growth (Dentelli et al, 2004; Dentelli et al, 2011). We provide a proof of concept, in the present study, for the proangiogenic properties of TEC-derived EVs as well. This observation indicates that, as in normal ECs exposed to inflammatory stimuli (Lombardo et al, 2016), EVs released by TECs can act locally as paracrine proangiogenic mediators. An anti-IL-3R blocking antibody (He et al, 2015) was therefore used to investigate whether IL-3R blockade can be therapeutically effective in preventing and/or impairing the growth of tumor vessels that have already formed by interfering with TEC-derived EVs. This may well be quite significant as an efficient blood supply is required for cancer cells to grow beyond a critical mass and progress to a malignant phenotype (Gomes et al, 2013; Lee et al, 2015). Indeed, we have proven that anti-IL-3R-EVs, besides preventing the formation of tumor vessels *in-vivo*, are also able to impair the growth of TEC-derived tumor vessels. EVs are known to influence the behavior of other cells by transferring lipids, proteins, mRNAs, transcription factors and (Valadi et al, 2007; Deregibus et al, 2007; Camussi et al, 2010; Lee et al, 2012; Tickner et al, 2014). This action suggests that IL-3R blockade somehow alters EV biological activity by changing their cargo. Genome-wide profiling has revealed that miRs are frequently abnormally expressed in human cancers (D'Angelo et al, 2016; Takahashi et al, 2017). Moreover, it is known that miRs are involved in tumorigenesis, metastasis, chemo-resistance and angiogenesis (Wang et al, 2015; D'Angelo et al, 2016; He et al, 2016; Takahashi et al, 2017). TEC-derived EVs were therefore analyzed for their miR cargo. Indeed, a number of modulated miRs, as compared to naïve EVs, were found in anti-IL-3R-EVs. There is an ever increasing amount of evidence to suggest that

miRs could work differentially in human tumors. In fact, context-dependent and target-dependent miR function has been reported (Gao et al, 2010). As the crucial biological regulators, miRs that act by suppressing their target genes are involved in a variety of pathophysiological processes. It is generally accepted that miRs are often dysregulated in many types of neoplasm and other human diseases. In cancer diseases, miRs may function as oncogenes or tumor suppressors (Sun et al, 2013). As constitutive activation of the Wnt signaling pathway is a common feature of neoplasm and contributes to its development, progression and metastasis in various cancers, numerous studies have performed. They revealed that miR-mediated gene regulation are interconnected with the Wnt/β-catenin signaling pathway, forming a Wnt/β- catenin–miR regulatory network (Sun et al, 2013). Analyses of the pathways associated with anti-IL-3R-EV-miR expression/modulation have led us to the idea that some may potentially play a critical role in our model. Attention was focused on miRs involved in the regulation of the Wnt/β-catenin signaling pathway in order to identify a crucial and less complex network of working in combination. The canonical Wnt/β-catenin pathway can be positively or negatively regulated by miRs at multiple levels (Sun et al, 2013; Ghahhari et al, 2015). As shown in this study, a number of carried miRs by anti-IL-3R-EVs are able to target the Wnt/β-catenin pathway (Sun et al, 2013; Ghahhari et al, 2015). Two of these, miR-214-3p, which directly targets β-catenin (Wang et al, 2012) and miR-24-3p, which targets two members of the "β-catenin interacting complex" (APC and GSK3β) (Pillai et al, 2014) were chosen for study. The "destruction complex" controls the stability of cytoplasmic β-catenin. When the Wnt pathway is not engaged, CK1 and GSK3β phosphorylate Axin-bound β-catenin to drive β-catenin to the proteasome for disruption. In this study, we demonstrate that APC and GSK3β as well as S33-S37-phosphorylated β-catenin content increased in TECs as the result of anti-IL-3R-EV treatment. Such specific phosphorylated sequence, at the N-terminal domain of β-catenin, corresponds to the consensus β-TrCP recognition site required for SCF β-TrCP E3 ubiquitin ligase-mediated degradation (Marikawa et al, 1998; Kitagawa M et al, 1999; Hart M et al, 1999). We herein provided evidences for the formation of a pβ-catenin/β-TrCP complex as the result of anti-IL-3R-

EV treatment. Moreover, it is demonstrated that the effects of anti-IL-3R-EVs may be recapitulated by transfecting cells with antago-miR-24-3p-EVs or using EVs that are depleted of miR-24-3p to stimulate TECs. Furthermore, the transfection of TECs with pre-miR-214-3p and the treatment of TECs with EVs that over-express miR-214-3p led to a reduction in β-catenin content. The same effects were observed upon anti-IL-3R-EV treatment. β-catenin, in the nucleus, functions as a transcription factor to activate the expression of cell proliferation, migration and survival genes, such as c-myc and cyclin D1 (Kiewisz e al, 2015; Song et al, 2015; Bastakoty et al, 2016; Yang et al, 2016). c-myc was found to be upregulated in naïve EV-treated TECs, whereas it was downregulated in TECs stimulated with anti-IL-3R-EVs, antago-miR-24-3p-EVs and pre-miR-214-3p-EVs, which is consistent with what is known on the integrated miR-24-3p and miR-214-3p interaction-network. c-myc is involved in the regulation of proliferation, growth, differentiation and cell survival. It also plays a role in vascular maturation and stabilization, as it is involved in vasculogenesis and angiogenesis (Baudino et al, 2002; Florea et al, 2013; Chang et al, 2016). c-myc has often been found to be deregulated and/or overexpressed in transformed cells. Our findings suggest that EVs may contribute to c-myc deregulation, even in tumor vessels, via epigenetic mechanisms that target the Wnt/β-catenin pathway.

The growing amount of information available on the Wnt/β-catenin regulatory network points to the existence of a complex circuit in cancer cells (Hoffmeyer et al, 2012; Ghahhari et al, 2015; Liu et al, 2016). An analysis of the modulated miRs in anti-IL-3R-EVs uncovered many predictable miRs which post-transcriptionally control the Wnt/β-catenin pathway at different levels, including miR-200a, miR-126, miR-130 and many others (Mongroo et al, 2010; Schepeler et al, 2012; Hoffmeyer et al, 2012; Sun et al, 2013; Ghahhari et al, 2015; Liu et al, 2016). Although we cannot exclude the possibility that EV inducing effects may depend largely on the combination of all together, a comparison of the miRs carried by antago-miR-24-3p-EVs, pre-miR-214-3p-EVs, anti-IL-3R-EVs and their functional activity would appear to point to the crucial role played by

selective enrichment pathways. As a matter of fact, antago-miR-24-3p-EVs, which were enriched in miR-214-3p, were also much more effective in their antiangiogenic action than pre-miR-214-3p-EVs. Moreover, a further and deeper comparison among pre-miR-214-3p-EV, antago-miR-24-3p-EV and anti-IL-3R-EV miR content led us to hypothesize that their overlapping anti-angiogenic effects might also depend on the combined action of a pattern of shared miRs (miR-222-3p, miR-16-5p, miR-484 for all EV samples; miR-19b-3p miR-17-5p, miR-196b-5p, miR-365b-5p for pre-miR-214-3p-EVs and anti-IL-3R-EVs; miR-106a-5p, miR-197-3p, miR-193b-3p for antago-miR-24-3p-EVs and anti-IL-3R-EVs) which may be involved in the regulation of a network of genes related to cancer development/progression. Moreover, we found that miR-16-5p, commonly shared by pre-miR-214-3p-EVs, antago-miR-24-3p-EVs, and in anti-IL-3R-EVs significantly correlated with 4 out of the 5 pathways identified by DIANA miR path software. Finally, our results suggest that miR-24-3p may be involved in the reverse epigenetic silencing of miR-214-3p, which moves to EVs from cells. Therefore, besides supporting the notion that silencing or deleting miRs widely modifies the cellular miR network, our results also raise additional concerns about using antago-miRs as therapeutics (Dai et al, 2015).

The transfer of EV-miR cargo into recipient cells is a potent mechanism that can support cancer cell survival and/or promote angiogenesis (Grange et al, 2011; Penfornis et al, 2016; Takahashi et al, 2017). We herein provide evidence to show that, just like tumor cells, EVs released from TECs acquire unique miR-cargo features which account for their paracrine mechanism of action. We also identify the Wnt/β-catenin pathway as a crucial regulator of TEC-derived EV proangiogenic action. Moreover, our data indicate that the IL-3R blockade may be a pharmacological option that interferes with TEC-derived EV proangiogenic action. Finally, there is clear interest in combining miR therapeutics, delivered by small-carriers with conventional cytotoxic agents, and molecularly targeted drugs (Dai et al, 2015). The IL-3R blockade may have the advantage of combining standard-of-care treatments with an already established and efficient EV-miR package which can enhance antitumor effects.

REFERENCES

Baker NE. Transcription of the segment-polarity gene wingless in the imaginal discs of Drosophila, and the phenotype of a pupal-lethal wg mutation. *Development* 1988; **102:** 489-497

Baluk P, Morikawa S, Haskell A, Mancuso M, McDonald DM. Abnormalities of basement membrane on blood vessels and endothelial sprouts in tumors. *Am J Pathol* 2003; **163:** 1801–1815.

Bao B, Ali S, Kong D, Sarkar SH, Wang Z, Banerjee S et al. Anti-Tumor Activity of a Novel Compound-CDF Is Mediated by Regulating miR-21, miR-200, and PTEN in Pancreatic Cancer. *PLoS One* 2011; **3:** e17850.

Bastakoty D, Young PP. Wnt/β-catenin pathway in tissue injury: roles in pathology and therapeutic opportunities for regeneration. *FASEB J* 2016; **30**: 3271-3284.

Baudino TA, McKay C, Pendeville-Samain H, Nilsson JA, Maclean KH, White EL, *et al.* c-Myc is essential for vasculogenesis and angiogenesis during development and tumor progression. *Genes Dev* 2002 **1**: 2530-2543.

Boll K, Reiche K, Kasack K, Morbt N, Kretzschmar AK, Tomm JM, et al. MiR-130a, miR-203 and miR-205 jointly repress key oncogenic pathways and are downregulated in prostate carcinoma. *Oncogene* 2013; **3:** 277–285.

Brizzi MF, Dentelli P, Rosso A, Calvi C, Gambino R, Cassader M, *et al*. RAGE- and TGF-beta receptor-mediated signals converge on STAT5 and p21waf to control cell-cycle progression of mesangial cells: a possible role in the development and progression of diabetic nephropathy. *FASEB J* 2004; **18**: 1249–1251.

Brizzi MF, Formato L, Dentelli P, Rosso A, Pavan M, Garbarino G, *et al.* Interleukin-3 Stimulates Migration and Proliferation of Vascular Smooth Muscle Cells A Potential Role in Atherogenesis. *Circulation* 2001; **103**: 549-554.

Brizzi MF, Formato L, Dentelli P, Rosso A, Pavan M, Garbarino G, Pegoraro M, Camussi G, Pegoraro L. Interleukin-3 stimulates migration and proliferation of vascular smooth muscle cells: a potential role in atherogenesis. *Circulation* 2001; **103:** 549 –554.

Brizzi MF, Garbarino G, Rossi PR, Pagliardi GL, Arduino C, Avanzi GC, Pegoraro L. Interleukin 3 stimulates proliferation and triggers endothelial-leukocyte adhesion molecule 1 gene activation of human endothelial cells. *J Clin Invest* 1993; **91:** 2887-92.

Bruno S, Tapparo M, Collino F, Chiabotto G, Deregibus MC, Soares Lindoso R. Renal Regenerative Potential of Different Extracellular Vesicle Populations Derived from Bone Marrow Mesenchymal Stromal Cells. *Tissue Eng Part A* 2017.[Epub ahead of print]

Bussolati B, Deambrosis I, Russo S, Deregibus MC, Camussi G. Altered angiogenesis and survival in human tumor-derived endothelial cells. *FASEB J* 2003; **17**: 1159–1161.

Butler JM, Kobayashi H, Rafii S. Instructive role of the vascular niche in promoting tumour growth and tissue repair by angiocrine factors. *Nat Rev Cancer* 2010; **10:** 138–146.

Camussi G, Deregibus MC, Bruno S, Cantaluppi V, Biancone L. Exosomes/microvesicles as a mechanism of cell-to-cell communication. *Kidney Int* 2010; **78**: 838–848.

Carmeliet P. *Nat Med* 2003; **9:** 653–660.

Cavallari C, Ranghino A, Tapparo M, Cedrino M, Figliolini F, Grange C, *et al*. Serum-derived extracellular vesicles (EVs) impact on vascular remodeling and prevent muscle damage in acute hind limb ischemia. *Sci Rep* 2017; **7**: 8180.

Chang HC, Hsieh TH, Lee YW, Tsai CF, Tsai YN, Cheng CC, *et al.* c-Myc and viral cofactor Kaposin B co-operate to elicit angiogenesis through modulating miRNome traits of endothelial cells. *BMC Syst Biol* 2016; **10**: 1-16.

Chiurillo MA. Role of the Wnt/β-catenin pathway in gastric cancer: An in-depth literature review. *World J Exp Med* 2015; **5**: 84-102.

Clevers H, Nusse R. Wnt/β-catenin signaling and disease, *Cell* 2012; **149**: 1192-1205.

Clevers H. Wnt/beta-catenin signaling in development and disease. *Cell* 2006; **127:**469-480.

Coller HA, Grandori C, Tamayo P, Colbert T, Lander ES, et al. Expression analysis with oligonucleotide microarrays reveals that MYC regulates genes involved in growth, cell cycle, signaling, and adhesion. *Proc Natl Acad Sci U S A* 2000; **97:** 3260–3265.

Collino F, Pomatto M, Bruno S, Lindoso RS, Tapparo M, Sicheng W, *et al*. Exosome and Microvesicle-Enriched Fractions Isolated from Mesenchymal Stem Cells by Gradient Separation Showed Different Molecular Signatures and Functions on Renal Tubular Epithelial Cells. *Stem Cell Rev* 2017; **13**: 226-243.

Croce JC, McClay DR. Evolution of the Wnt pathways. Methods. *Mol Biol* 2008; **469:** 3-18.

Dai X, Tan C. Combination of microRNA therapeutics with small-molecule anticancer drugs: mechanism of action and co-delivery nanocarriers. *Adv Drug Deliv Rev* 2015; **81**: 184-197.

D'Angelo B, Benedetti E, Cimini A, Giordano A. MicroRNAs: A Puzzling Tool in Cancer Diagnostics and Therapy. *Anticancer Res* 2016; **36**: 5571-5575.

de Nigris F, Balestrieri ML, Napoli C. Targeting c-Myc, Ras and IGF cascade to treat cancer and vascular disorders. *Cell Cycle* 2006; **5:** 1621–1628.

Dentelli P, Del Sorbo L, Rosso A, Molinar A, Garbarino G, Camussi G, *et al*. Human IL-3 Stimulates Endothelial Cell Motility and Promotes In Vivo New Vessel Formation. *J Immunol* 1999; **163**: 2151-2159.

Dentelli P, Rosso A, Calvi C, Ghiringhello B, Garbarino G, Camussi G, *et al*. IL-3 affects endothelial cell-mediated smooth muscle cell recruitment by increasing TGF beta activity: potential role in tumor vessel stabilization. *Oncogene* 2004; **23**: 1681-1692.

Dentelli P, Rosso A, Garbarino G, Calvi C, Lombard E, Di Stefano P *et al*. The interaction between KDR and interleukin-3 receptor (IL-3R) beta common modulates tumor neovascularization. *Oncogene* 2005; **24**: 6394–6405.

Dentelli P, Rosso A, Olgasi C, Camussi G, Brizzi MF. IL-3 is a novel target to interfere with tumor vasculature. *Oncogene* 2011; **30**: 4930–4940.

Dentelli P, Rosso A, Orso F, Olgasi C, Taverna D, Brizzi MF. microRNA-222 controls neovascularization by regulating signal transducer and activator of transcription 5A expression. *Arterioscler Thromb Vasc Biol* 2010; **30**: 1562–1568.

Dentelli P, Trombetta A, Togliatto G, Zeoli A, Rosso A, Uberti B, *et al*. Formation of STAT5/PPAR{gamma} Transcriptional Complex Modulates Angiogenic Cell Bioavailability in Diabetes. *Arterioscler Thromb Vasc Biol* 2009; **29**: 114-120.

Deregibus MC, Cantaluppi V, Calogero R, Lo Iacono M, Tetta C, Biancone L, *et al*. Endothelial progenitor cell derived microvesicles activate an angiogenic program in endothelial cells by a horizontal transfer of mRNA. *Blood* 2007; **110**: 2440–2448.

Deregibus MC, Cantaluppi V, Doublier S, Brizzi MF, Deambrosis I, Albini A, *et al*. HIV-1-Tat protein activates phosphatidylinositol 3-kinase/ AKT-dependent survival pathways in Kaposi's sarcoma cells. *J Biol Chem* 2002; **277**: 25195-25202.

Djuranovic S, Nahvi A, Green R.A. Parsimonious Model for Gene Regulation by miRNAs. *Science* 2011; **331**:550-553.

Ferrara N. Molecular and biological properties of vascular endothelial growth factor. *J Mol Med* 1999; **77:** 527–543.

Florea V, Bhagavatula N, Simovic G, Macedo FY, Fock RA, Rodrigues CO. c-Myc is essential to prevent endothelial pro-inflammatory senescent phenotype. *PLoS One* 2013; **8:** e73146.

Folkman J, Watson K, Ingber D, Hanahan D. Induction of angiogenesis during the transition from hyperplasia to neoplasia. *Nature* 1989; **339:** 58-61.

Folkman J. Angiogenesis: an organizing principle for drug discovery? Nat Rev Drug Discov. 2007; **6:** 273–286.

Fuchs SY, Spiegelman VS, Kumar KG. The many faces of beta-TrCP E3 ubiquitin ligases: reflections in the magic mirror of cancer. *Oncogene* 2004; **23**: 2028-2036.

Gacche RN, Meshram RJ. Targeting tumor micro-environment for design and development of novel anti-angiogenic agents arresting tumor growth. *Progr Biophys Mol Biol* 2013; **113:** 333-354.

Gallo S, Gili M, Lombardo G, Rossetti A, Rosso A, Dentelli P, *et al.* Stem Cell-Derived, microRNA-Carrying Extracellular Vesicles: A Novel Approach to Interfering with Mesangial Cell Collagen Production in a Hyperglycaemic Setting. *PLoS One* 2016; **11**: e0162417.

Gao FB. Context-dependent functions of specific microRNAs in neuronal development. *Neural Dev* 2010; **5**: 25.

Ghahhari NM, Babashah S. Interplay between microRNAs and WNT/β-catenin signalling pathway regulates epithelial-mesenchymal transition in cancer. *Eur J Cancer* 2015; **51**: 1638-1649.

Giusti I, Delle Monache S, Di Francesco M, Sanità P, D'Ascenzo S, Gravina GL, *et al*. From glioblastoma to endothelial cells through extracellular vesicles: messages for angiogenesis. *Tumor Biol* 2016; **37**: 12743–12753.

Gomes FG, Nedel F, Alves AM, Nör JE, Tarquinio SB. Tumor angiogenesis and lymphangiogenesis: tumor/endothelial crosstalk and cellular/microenvironmental signaling mechanisms. *Life Sci* 2013; **92**: 101-107.

Grange C, Bussolati B, Bruno S, Fonsato V, Sapino A, Camussi G. Isolation and characterization of human breast tumor derived endothelial cells. *Oncol Rep* 2006; **15**: 381–386.

Grange C, Tapparo M, Collino F, Vitillo L, Damasco C, Deregibus MC, *et al*. Microvesicles released from human renal cancer stem cells stimulate angiogenesis and formation of lung premetastatic niche. *Cancer Res* 2011; **71**: 5346-5356.

Greenberger JS, Eckner RJ, Sakakeeny M, Marks P, Reid D, Nabel G *et al*. Interleukin 3-dependent hematopoietic progenitor cell lines. *Fed Proc* 1983; **42**: 2762–2771.

Hart M, Concordet JP, Lassot I, Albert I, del los Santos R, Durand H, *et al.* The F-box protein beta-TrCP associates with phosphorylated beta-catenin and regulates its activity in the cell. *Curr Biol* 1999; **9**: 207-210.

He M, Zhou W, Li C, Guo M. MicroRNAs, DNA Damage Response, and Cancer Treatment. *Int J Mol Sci* 2016; **17:** E2087.

He SZ, Busfield S, Ritchie DS, Hertzberg MS, Durrant S, Lewis ID, *et al*. A Phase 1 study of the safety, pharmacokinetics and anti-leukemic activity of the anti-CD123 monoclonal antibody CSL360 in relapsed, refractory or high-risk acute myeloid leukemia. *Leuk Lymphoma* 2015; **56**: 1406-1415.

Hoffmeyer K, Raggioli A, Rudloff S, Anton R, Hierholzer A, Del Valle I, *et al*. Wnt/β-catenin signaling regulates telomerase in stem cells and cancer cells. *Science* 2012; **336**: 1549-1554.

Huang K, Zhang JX, Han L, You YP, Jiang T, Pu PY, Kang CS. MicroRNA roles in beta-catenin pathway. *Mol Cancer* 2010; **9:** 252

Ihle, J.N. Interleukin-3 and hematopoiesis. *Chem Immunol* 1992; **51**: 65–106.

Kerbel RS. Tumor angiogenesis. *N Engl JMed* 2008; **358:** 2039–2049.

Kharaziha P, Ceder S, Li Q, Panaretakis T. Tumor cell-derived exosomes: a message in a bottle. *Biochimic Biophys Acta* 2012; **1826**: 103-111.

Kiewisz J, Wasniewski T, Kmiec Z. Participation of WNT and β-Catenin in Physiological and Pathological Endometrial Changes: Association with Angiogenesis. *BioMed Research International* 2015; **2015**: 854056.

Kitagawa M, Hatakeyama S, Shirane M, Matsumoto M, Ishida N, Hattori K, *et al.* An F-box protein, FWD1, mediates ubiquitin-dependent proteolysis of beta-catenin. *EMBO J* 1999; **18**: 2401-2410.

Koenig W, Khuseyinova N. Biomarkers of atherosclerotic plaque instability and rupture. *Arterioscler Thromb Vasc Biol* 2007; **27:** 15–26.

Korpelainen EI, Gamble JR, Vadas MA, Lopez AF. IL-3 receptor expression, regulation and function in cells of the vasculature. *Immunol Cell Biol* 1996; **74:** 1-7

Lee E, Pandey NB, Popel AS. Crosstalk between cancer cells and blood endothelial and lymphatic endothelial cells in tumour and organ microenvironment. *Expert Rev Mol Med* 2015; **17:** e3.

Lee Y, El Andaloussi S, Wood MJ. Exosomes and microvesicles: extracellular vesicles for genetic information transfer and gene therapy. *Hum Mol Genet* 2012; **21**: R125–R134.

Lin H, Fang Z, Su Y, Li P, Wang J, Liao H, *et al*. DHX32 Promotes Angiogenesis in Colorectal Cancer Through Augmenting β-catenin Signaling to Induce Expression of VEGFA. *EBioMedicine* 2017; **18**: 62-72.

Liu N, Zhou N, Chai N, Liu X, Jiang H, Wu Q, *et al*. Helicobacter pylori promotes angiogenesis depending on Wnt/β-Catenin -mediated vascular endothelial growth factor via the cyclooxygenase-2 pathway in gastric cancer. *BMC Cancer* 2016; **16**: 321.

Logan CY, Nusse R. The Wnt signaling pathway in development and disease. *Annu Rev Cell Dev Biol* 2004; **20:** 781-810.

Lombardo G, Dentelli P, Togliatto G, Rosso A, Gili M, Gallo S, *et al*. Activated Stat5 trafficking Via Endothelial Cell-derived Extracellular Vesicles Controls IL-3 Pro-angiogenic Paracrine Action. *Sci Rep* 2016; **6:** 25689**.**

Marikawa Y, Elinson RP. beta-TrCP is a negative regulator of Wnt/beta-catenin signaling pathway and dorsal axis formation in Xenopus embryos. *Mech Dev* 1998; **77**: 75-80.

Mestdagh P, Van Vlierberghe P, De Weer A, Muth D, Westermann F, Speleman F, Vandesompele J. A novel and universal method for microRNA RT-qPCR data normalization. *Genome Biol* 2009; **10**: R64.

Metcalf D, Begley CG, Johnson GR, Nicola NA, Lopez AF, Williamson DJ. Effects of purified bacterially synthesized murine multi-CSF (IL-3) on hematopoiesis in normal adult mice. *Blood* 1986; **68:** 46–57.

Miki T, Yasuda SY, Kahn M. Wnt/β-catenin signaling in embryonic stem cell self-renewal and somatic cell reprogramming. *Stem Cell Rev* 2011; **7**: 836-846.

Miller JR. The Wnts. *Genome Biol* 2002; **3:** REVIEWS3001

Moldenhauer LM, Cockshell MP, Frost L, Parham KA, Tvorogov D, Tan LY *et al*. Interleukin-3 greatly expands non-adherent endothelial forming cells with pro-angiogenic properties. *Stem Cell Res* 2015; **14**: 380–395.

Mongroo PS, Rustgi AK. The role of the miR-200 family in epithelial-mesenchymal transition. *Cancer Biol Ther* 2010; **10**: 219-222.

Napoli C, Lerman LO, de Nigris F, Sica V. c-Myc oncoprotein: a dual pathogenic role in neoplasia and cardiovascular diseases? *Neoplasia* 2002; **4:** 185–190.

Newby AC, Zaltsman AB. Fibrous cap formation or destruction: the critical importance of vascular smooth muscle cell proliferation, migration and matrix formation. *Cardiovasc Res* 1999; **41:** 345–360.

Packard RR, Libby P. Inflammation in atherosclerosis: from vascular biology to biomarker discovery and risk prediction. *Clin Chem* 2008; **54:** 24–38.

Pelengaris S, Khan M. The many faces of c-MYC. *Arch Biochem Biophys* 2003; **416:** 129–136.

Penfornis P, Vallabhaneni KC, Whitt J, Pochampally R. Extracellular vesicles as carriers of microRNA, proteins and lipids in tumor microenvironment. *Int J Cancer* 2016; **138**: 14-21.

Pillai MM, Gillen AE, Yamamoto TM, Kline E, Brown J, Flory K, *et al*. HITS-CLIP reveals key regulators of nuclear receptor signaling in breast cancer. *Breast Cancer Res Treat* 2014; **146**: 85-97.

Rafii S, Lyden D, Benezra R, Hattori K, Heissig B. Vascular and haematopoietic stem cells: novel targets for anti-angiogenesis therapy? *Nat Rev Cancer* 2002; **2:** 826-35.

Ross R. Atherosclerosis: an inflammatory disease. *N Engl J Med* 1999; **340:** 115–123.

Rothenberg ME, Owen WF Jr, Silberstein DS, Woods J, Soberman RJ, Austen KF *et al*. Human eosinophils have prolonged survival, enhances functional properties, and become hypodense when exposed to human interleukin 3. *J Clin Invest* 1988; **81**: 1986–1992.

Sadowski HB, Shuai K, Darnell JE Jr, Gilman MZ. A common nuclear signal transduction pathway activated by growth factor and cytokine receptors. *Science* 1993; **261**: 1739–1744.

Saini S, Majid S, Yamamura S, Tabatabai L, Suh SO, Shahryari V, et al. *Clin Cancer Res* 2011; **16**: 5287–5298

Sceneay J, Smyth MJ, Moller A. The pre-metastatic niche: finding common ground. *Cancer Metastasis Rev* 2013; **32**: 449–464.

Schepeler T, Holm A, Halvey P, Nordentoft I, Lamy P, Riising EM, *et al.* Attenuation of the beta-catenin/TCF4 complex in colorectal cancer cells induces several growth-suppressive microRNAs that target cancer promoting genes. *Oncogene* 2012; **31**: 2750-2760.

Shchors K, Evan G. Tumor angiogenesis: cause or consequence of cancer? *Cancer Res* 2007. **67:** 7059–7061.

Song X, Xin N, Wang W, Zhao C. Wnt/β-catenin, an oncogenic pathway targeted by H. pylori in gastric carcinogenesis. *Oncotarget* 2015; **6**: 35579–35588.

Spano D, Zollo M. Tumor microenvironment: a main actor in the metastasis process. *Clin Exp Metastasis* 2012; **29**: 381–395.

St Croix B, Rago C, Velculescu V, Traverso G, Romans KE, Montgomery E et al. Genes expressed in human tumor endothelium. *Science* 2000; **289:** 1197–1202.

Sun X, He Y, Huang C, Ma TT, Li J. Distinctive microRNA signature associated of neoplasms with the Wnt/β-catenin signaling pathway. *Cell Signal* 2013; **25**: 2805-2811.

Takahashi RU, Prieto-Vila M, Hironaka A, Ochiya T. The role of extracellular vesicle microRNAs in cancer biology. *Clin Chem Lab Med* 2017; **55**: 648-656.

Tickner JA, Urquhart AJ, Stephenson SA, Richard DJ, O'Byrne KJ. Functions and therapeutic roles of exosomes in cancer. *Front Oncol* 2014; **4**: 127.

Togliatto G, Dentelli P, Gili M, Gallo S, Deregibus C, Biglieri E, *et al*. Obesity reduces the pro-angio-genic potential of adipose tissue stem cell-derived extracellular vesicles (EVs) by impairing miR-126 content: impact on clinical applications. *Int J Obes* 2016; **40**: 102–111.

Trombetta A, Togliatto G, Rosso A, Dentelli P, Olgasi C, Cotogni P, *et al.* Increase of palmitic acid concentration impairs endothelial progenitor cell and bone marrow-derived progenitor cell bioavailability: role of the STAT5/PPARγ transcriptional complex. *Diabetes* 2013; **62**: 1245-1257.

Uberti B, Dentelli P, Rosso A, Defilippi P, Brizzi MF. Inhibition of b1 integrin and IL-3Rb common subunit interaction hinders tumour angiogenesis. *Oncogene* 2010; **29:** 6581–6590.

Valadi H, Ekstrom K, Bossios A, Sjostrand M, Lee JJ, Lotvall JO. Exosome-mediated transfer of mRNAs and microRNAs is a novel mechanism of genetic exchange between cells. *Nat Cell Biol* 2007; **9**: 654-659.

Viticchie G, Lena AM, Latina A, Formosa A, Gregersen LH, Lund AH, Bernardini S et al. MiR-203 controls proliferation, migration and invasive potential of prostate cancer cell lines. *Cell Cycle* 2011; **10**: 1121–1131.

Vlachos IS, Zagganas K, Paraskevopoulou MD, Georgakilas G, Karagkouni D, Vergoulis T, *et al.* DIANA-miRPath v3.0: deciphering microRNA function with experimental support. *Nucleic Acids Res* 2015; **43**: W460-466.

Wang W, Zhang E, Lin C. MicroRNAs in tumor angiogenesis. *Life Sci* 2015; **136**: 28-35.

Wang X, Chen J, Li F, Lin Y, Zhang X, Lv Z, *et al*. MiR-214 inhibits cell growth in hepatocellular carcinoma through suppression of β-catenin. *Biochem Biophys Res Commun* 2012; **428**: 525-531.

Wimperis, J. Z., C. M. Niemeyer, C. A. Sieff, B. Mathey-Prerot, D. G. Nathan, and R. J. Arceci. Granulocyte-macrophage colony-stimulating factor and interleukin-3 mRNA are produced by a small fraction of blood mononuclear cells. *Blood* 1989; **74:** 1525-1530.

Xia H, Ooi LL, Hui KM. MiR-214 targets β-catenin pathway to suppress invasion, stem-like traits and recurrence of human hepatocellular carcinoma. *PLoS One* 2012; **9:** e44206.

Xu M and Mo YY. The Akt-associated microRNAs. *Cell Mol Life Sci* 2012; **69:** 3601-12

Yang K, Wang X, Zhang H, Wang Z, Nan G, Li Y, *et al*. The evolving roles of canonical WNT signaling in stem cells and tumorigenesis: implications in targeted cancer therapies. *Lab Invest* 2016; **96**: 116-136.

Zeoli A, Dentelli P, Rosso A, Togliatto G, Trombetta A, Damiano L *et al*. Interleukin-3 promotes expansion of hemopoietic-derived CD45+ angiogenic cells and their arterial commitment via STAT5 activation. *Blood* 2008; **112:** 350–361.

Zhang B, Wu X, Zhang X, Sun Y, Yan Y, Shi H, *et al*. Human Umbilical Cord Mesenchymal Stem Cell Exosomes Enhance Angiogenesis Through the Wnt4/ β-Catenin Pathway. *Stem Cells Transl Med* 2015; **4**: 513–522.